FORMATION AND DETECTION OF ULTRAVIOLET INDUCED THYMINE DIMERS AND CONSTRUCTION OF NOVEL DEVICES

A Thesis

by

ANUSHKA NAGPAL

Submitted to the Office of Graduate and Professional Studies of
Texas A&M University
in partial fulfillment of the requirements for the degree of

MASTER OF SCIENCE

Chair of Committee,	Peter Rentzepis
Committee Members,	Jun Kameoka
	Kevin Nowka
	Shuhua Yuan
Head of Department,	Miroslav Begovic

August 2021

Major Subject: Electrical Engineering

ABSTRACT

In this study, thymine dimers were detected, for the first time, in both thymine and DNA aqueous solutions using Raman spectroscopy. Thymine dimers, formed by UV radiation of DNA, inactivate bacteria by inhibiting their DNA replication. UV inactivation of bacteria is becoming increasingly important because the number of antibiotic-resistant bacteria is increasing. It is found that the formation of these dimers continues to increase for 20 minutes of irradiation, after which an equilibrium is established between the thymine monomers and dimers. In addition, the formation of another mutagenic photoproduct, (6-4) photoproduct was identified by its fluorescence spectrum. The spectroscopic methods used in this study pave the way for fast and definite identification of the ratio of live and dead bacteria and thus become more advantageous than traditional techniques such as plating.

Owing to the fact that, in many cases, the in-situ detection of different material(s) is imperative, we have designed, constructed, and utilized various hand-held instruments which are capable of recording and displaying the spectra of the investigated materials, and even biological molecules, in-situ within minutes. We have designed and constructed a hand-held device that records resonance Raman spectra of bacterial carotenoids and allows us to measure the ratio of live and dead bacteria after UV irradiation, and also identify various bacterial strains. Another hand-held device was constructed which when used with a telescope, can detect remotely the percentage of inactivated bacteria after UV irradiation, by measuring the change in fluorescence intensity of tryptophan and tyrosine. Both of these devices were constructed and operated successfully. We have also designed and constructed another handheld instrument that uses a cell-

phone camera to detect Raman and fluorescence spectra of various chemicals and biological molecules.

We developed a technique to expand human vision to UV and infrared (IR) regions, by making use of IR to visible upconverting rare-earth-doped microparticles (NaYF4:Yb,Er), and a UV to visible converting fluorescent dye (Stilbene 420). These particles were embedded in proteins and rod outer segments in order to successfully demonstrate the conversion. We also developed an eyeglass device, in which the fluorescent dye and upconverting microparticles were dispersed in the lens to expand the visual region of the human eye.

DEDICATION

Dedicated to

My grandfather, Mr. Om Prakash Walecha,

My mother, father, and sister

For their constant support, love, and encouragement

ACKNOWLEDGEMENTS

Firstly, I would like to thank my research advisor and committee chair, Dr. Peter Rentzepis, for his expert guidance, and support in the course of this research. I am thankful for the frequent and useful discussions I had with him, which enabled me to overcome many roadblocks in this research. He not only taught me to question every aspect of the research but at the same time imparted important life lessons. His support, both intellectual and emotional, were the primary factors that drove me into the completion of this thesis. I would also like to express my sincere gratitude to my committee members, Dr. Jun Kameoka, Dr. Kevin Nowka, and Dr. Shuhua Yuan, for their guidance.

Special thanks to my colleagues, Dinesh, Runze, and Arjun.

Finally, I would like to thank my mother and father, who have supported me in all my endeavors. Their constant support, encouragement, and love has always motivated me to push harder and achieve my goals. Thanks to my sister for always looking out for me and for supporting me every step of the way. Thanks to my grandfather for showering me with his love and blessings. Lastly, thanks to all my friends, for their support.

CONTRIBUTORS AND FUNDING SOURCES

Contributors

This work was supervised by Dr. Peter Rentzepis of the Department of Electrical and Computer Engineering.

Arjun Krishnamoorthi helped in conducting absorption and fluorescence measurements for thymine and DNA samples. Dinesh Dhankhar helped in the design and construction of the handheld instruments, and in the design and analysis of the upconverting particles experiments.

All other work conducted, for this thesis, was conducted by the student independently.

Funding Sources

This work was supported in part by the Air Force Office of Scientific Research (AFOSR) under Grant No. FA9550-20-1-0139, the Welch Foundation under Grant No. 1501928, and the Texas A&M Engineering Experiment Station (TEES). Its contents are solely the responsibility of the authors and do not necessarily represent the official views of AFOSR, Welch Foundation, or TEES.

TABLE OF CONTENTS

LIST OF FIGURES

Page

LIST OF TABLES

CHAPTER I

INTRODUCTION TO THE THESIS

Bacterial resistance to antibiotics has become a global health hazard. The prolonged presence of antibiotic drugs in their environment can cause bacteria to develop resistance mechanisms to antibiotics by producing enzymes that can destroy the drugs or restricting access to the bacteria by limiting or changing the entryways (1). In 2019, the U.S. Centers for Disease Control and Prevention (CDC) reported that more than 2.8 million antibiotic-resistant infections resulted in over 35,000 deaths in the United States, per year (2). Many of these infections often develop and spread in hospitals and other health care facilities, where most patients are prescribed antibiotic drugs which results in antibiotic-resistant infections reaching the most vulnerable patients (3). It is well known that ultraviolet (UV) light has germicidal properties because it inhibits bacterial DNA replication by the formation of thymine dimers in the DNA strands (4). Therefore, it is important to improve our understanding of this mechanism and develop techniques that can inactivate bacteria, especially on contaminated surfaces in health care facilities.

In this study, thymine dimers were formed by UV irradiation, of both thymine and DNA solutions, and were detected, for the first time, by Raman spectroscopy. A hand-held device that collects the resonance Raman spectra was also constructed that could be used in hospitals for in-situ detection of the percentage of bacteria inactivated after UV irradiation. We have also designed, constructed, operated, and patented another handheld instrument capable of detecting the Raman and fluorescence spectra of various chemicals and biological molecules. This device uses a transmission grating and a cell phone camera to detect the Raman light intensities emanating from

the sample, excited by a laser diode. This Raman instrument can be used with many cell phones available in the market.

Previous studies, by our group, suggest that the change in fluorescence intensity of tryptophan and tyrosine can be used to determine the ratio of live and dead bacteria (5). To that effect, we have used this principle to construct another hand-held instrument that can detect remotely the fluorescence intensity of bacterial components shortly before and after UV irradiation.

While UV light can be harmful to many organisms, UV vision can provide advantages such as finding food or hiding from a predator. To achieve UV and IR vision, we have developed a technique that expands the visual region of the human eye to 330 nm UV by using a fluorescent dye, Stilbene 420, and to near Infrared (IR) by using upconverting infrared to visible microparticles. The upconverting microparticles, Yb^{3+} and Er^{3+} are doped into a stable host lattice, $NaYF_4$. We also developed an eyeglass device by dispersing these IR microparticles in the lens, thus expanding the visual spectral range of the eye to UV and IR regions.

Chapter Format

Chapter II provides a brief overview of previous work on UV inactivation of bacteria, information on different spectroscopic techniques used in this study, and an introduction to two-photon Upconversion. Chapter III discusses the Materials and Methods used as well as the design and construction of the hand-held and eyeglass devices. The experimental results and the spectra obtained from the hand-held devices are discussed in Chapter IV. Chapter V provides a summary of this thesis and the scope of further improvements.

CHAPTER II

LITERATURE REVIEW AND INTRODUCTION TO SPECTROSCOPIC TECHNIQUES

Bacteria and Antibiotic resistance

Bacteria are single-celled prokaryotes and their nucleoid, which consists of their genetic material, does not have a nuclear membrane. Bacteria are widely believed to be the oldest living organisms on the planet (6). They can easily adapt to changing environments and can live in harsh environments such as extreme cold and heat, where multi-cellular organisms might cease to exist. Bacteria usually co-exist with living organisms, and either develop a mutualistic or parasitic relationship with their hosts. Bacteria, living inside living organisms, are essential for digesting food and fighting disease-causing bacteria in exchange for a hospitable living environment and food. Such bacteria are in a mutualistic relationship with the host. There are trillions of bacteria living on the skin and inside the human body. Bacteria that cause harm to the hosts while benefiting from them are said to be in a parasitic relationship with their hosts. These bacteria often cause diseases such as tuberculosis, meningitis, and food poisoning.

Most bacterial cells consist of a gel-like fluid called cytoplasm, which contains nucleoid and ribosomes. The nucleoid does not have a membrane, and it is defined as the region of the cytoplasm which consists of the DNA strands. Ribosomes are minute and free-floating particles that are responsible for the synthesis of proteins in the cell. In bacteria, they can be found in

quantities of thousands to tens of thousands. The cytoplasm is surrounded by a cell envelope, which consists of a cytoplasmic membrane, cell wall and outer capsule. The capsule consists of outward projections including flagella, which enables the bacterium to move, and pili, which helps the bacteria to attach itself to other hosts. Table 1 shows the chemical composition of a typical bacterial cell.

Table 1. Structural and chemical composition of a typical bacterial cell

Structure	**Composition**	**Reference**
Flagella	Proteins	(7)
Pili	Proteins	(8, 9)
Capsule (not always present)	Polysaccharide	(10)
Cell wall	Peptidoglycan	(11)
Cytoplasmic membrane	Proteins and phospholipids	(12)
Ribosomes	DNA and proteins	(13)
Nucleoid	DNA	(14)

Bacterial infections are treated with antibiotics, that either directly damages the cell wall, or inhibit nutrients from reaching the bacteria, thus slowing down their reproduction and eventually causing cell death. Antibiotics have been extensively used to cure bacterial infections since the 1940s. During the same period, it was observed that bacteria have started developing resistance against antibiotics (15). This resistance is caused due to two main reasons, nonessential and excessive use of antibiotics and non-completion of the recommended, needed antibiotic dose

(1). This increases the probability for the bacteria to develop antibiotic resistance by either making proteins that damage the antibiotic drug or by blocking pathways that inhibit the entry of the drug into the cell. Antibiotic-resistant bacteria have thus been increasing and now put a vast population at the risk on life-threatening antibiotic-resistant infections.

Ultraviolet Inactivation of Bacterial Cells

Since the early 1960s, considerable scientific research efforts have been focused on understanding the germicidal effect of UV light, specifically UV-C light which lies within the wavelength range of 100 – 280 nm (16-19). This germicidal effect is most efficient at 260 nm because it corresponds to the absorption maximum of the nitrogenous bases, also known as nucleobases, in DNA and RNA. DNA consists of a helical sugar-phosphate backbone which is connected to these nucleobases. The nucleobases are classified as purines and pyrimidines. The purine bases are Adenine (A) and Guanine (G), and the pyrimidine bases are Cytosine (C) and Thymine (T). The double-helical structure of the DNA arises due to the formation of hydrogen bonds between A-T and G-C of two different strands.

Ultraviolet light has many harmful effects on DNA, including strand breaks, deamination, oxidative mutations, and dimer formation (20). It has been proposed that the inactivation of bacteria occurs due to the formation of cyclobutane thymine dimers in DNA (4). These dimers are formed when the double bond of the thymine molecule dissociates, when irradiated with UV light, and forms a single covalent bond between adjacent thymine molecules located on the same DNA

strand, as shown in Figure 1 (B). As a result, these dimers cause the dissociation of hydrogen bonds between the two helical strands, thus inhibiting DNA replication, which causes bacterial death (17).

Studies have also shown the formation of other photoproducts, including the thymine (6-4) photoproduct, T-C dimers, and thymine cytosine (6-4) photoproducts, however, they were formed in much smaller yields than the thymine dimers (19, 21, 22). Purine bases are more resistant to UV light, with adenine dimers being formed at much lower yields (23). Figure 1 (A) depicts the structure of thymine monomer, thymine dimer, and (6-4) photoproduct.

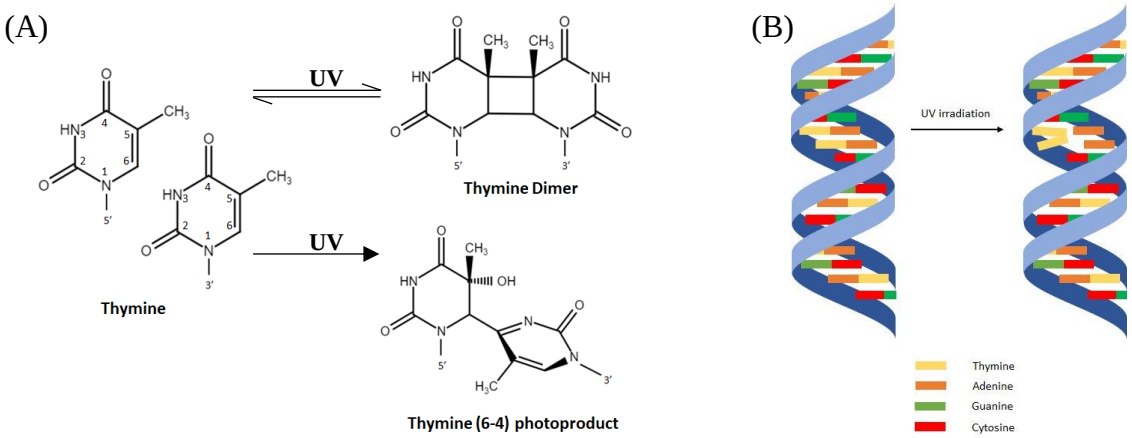

Figure 1. Structure of thymine, thymine dimer, and (6-4) photoproduct (A), and formation of UV-induced thymine dimers in DNA (B). Reprinted with permission from (24).

The formation of thymine dimers, in thymine solution, is carried out by irradiating frozen thymine solution. It has been reported that during the process of freezing the thymine solution, the water molecules crystallize together, leaving behind a concentrated thymine solution (25). This

concentrated thymine solution freezes to form a thymine monohydrate crystal, in which the thymine molecules are stacked on top of one another, which is the ideal structural position for dimerization (26).

Previous studies by our group have successfully demonstrated the effect of UV irradiation on tryptophan and tyrosine attached to the membrane of bacteria (5). It has been shown that the decrease in fluorescence intensity can provide a measure of the percentage of bacteria inactivated after UV irradiation. This principle is utilized by a handheld device for the remote detection of the ratio of inactivated bacteria in this research.

Fluorescence and Synchronous fluorescence spectroscopy

Fluorescence spectroscopy is a simple and versatile technique used to study the properties of fluorescent materials. When an atom or molecule is excited by light, the electrons are excited to a higher energy state. These electrons relax to the lowest vibrational state of the upper energy state via non-radiative transitions (phonon-phonon interactions) and fall back to different vibrational levels of the ground state, emitting photons of various frequencies. This is known as fluorescence. Figure 2 shows a diagram describing this process.

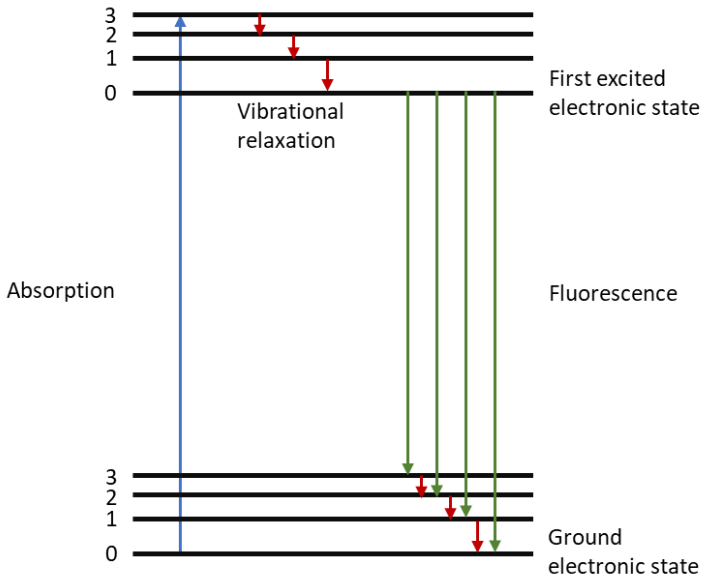

Figure 2. Jablonski diagram for fluorescence.

The fluorescence intensity of a molecule is measured by selecting an excitation wavelength and recording the emitted fluorescence wavelength in a particular wavelength interval.

Synchronous fluorescence spectroscopy has become increasingly popular for multi-component analysis. This technique measures the fluorescence of a sample, by synchronously changing the excitation and emission wavelengths such that the wavelength interval $\Delta\lambda$ between the two wavelengths remains constant. Using this technique, the fluorescence bands of different components in a mixture can be separated and studied independently. Figure 3 (1) shows the fluorescence bands of the tryptophan and tyrosine components in E. coli bacteria, while Figure 3 (2) and (3) show the synchronous fluorescence bands of tyrosine and tryptophan, respectively (5).

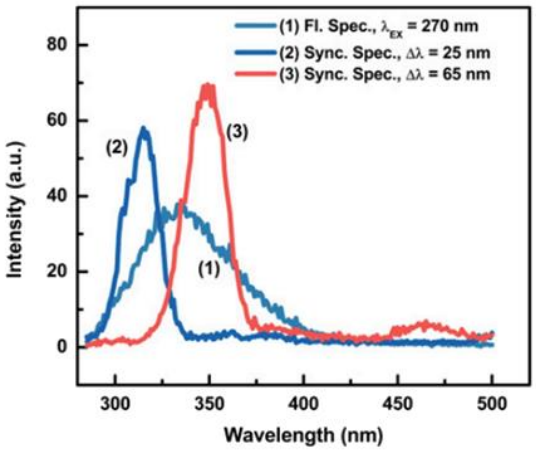

Figure 3. Normal and synchronous fluorescence spectra of E.coli in water (5).

Raman Spectroscopy

Raman spectroscopy is a popular spectroscopic technique used for the identification and characterization of different materials. It is based on the inelastic scattering of monochromatic light from a molecule. This phenomenon was first proposed theoretically by Adolf Smekal in 1923 (27) and was first observed experimentally by Chandrasekhara Venkata Raman and Kariamanikkam Srinivasa Krishnan in 1928 (28).

When light interacts with matter, it can either be absorbed or scattered. If monochromatic light is incident on a molecule, such that its frequency does not correspond to any absorption transition, a large portion of light passes through it. A small proportion of light will undergo scattering, such that most of the scattered light will have the same frequency as the incident beam. This is known as Rayleigh scattering. However, less than 0.001% of the scattered light will be scattered inelastically, with wavelengths either slightly higher or lower than that of the incident

light. This difference in wavelength arises due to the electromagnetic field polarizing the molecule and raising it to a short-lived virtual energy state. When the excited molecule reverts to a higher vibrational state of the ground state, a lower energy photon, than the incident photon, is emitted, called the Stokes scattering. However, if the molecule relaxes back to a lower vibration state, a higher energy photon is emitted, known as Anti-stokes scattering. Although both Stokes and Anti-Stokes scatterings have an equal probability of taking place, Stokes scattering is much more intense than Anti-Stokes. This arises due to the Boltzmann distribution which states that the energy states with lower energy have a higher probability of being occupied. Figure 4 shows a schematic diagram of Rayleigh, Stokes, and Anti-Stokes scattering.

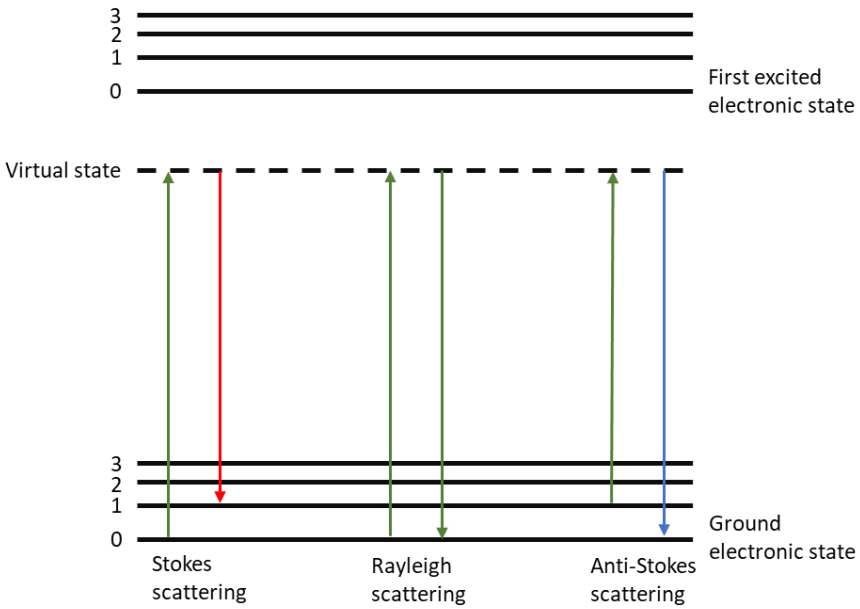

Figure 4. Schematic diagram of Rayleigh, Stokes, and Anti-Stokes scattering.

The Raman effect arises due to a change in polarizability of the molecule. Although the quantum mechanical description of this effect is more accurate, for simplicity, the classical description is discussed here. We consider a diatomic molecule and treat it like a mass on a spring. The vibration of this molecule can therefore be described by Hook's law as:

$$\mu \frac{d^2q}{dt^2} = -Kq,$$

where μ is the reduced mass of the molecule, and q is the total displacement.

This equation can be solved to obtain, $q = q_o \cos(2\pi \nu_m t)$ where ν_m is the frequency of vibration such that, $\nu_m = \frac{1}{2\pi}\sqrt{\frac{K}{\mu}}$.

Since the frequency of vibration depends on the bond strength and mass of atoms, it is evident that each molecular vibration will have its unique signature. An incident electric field with frequency ν_o will cause an induced dipole moment, M, in the molecule such that the M is a product of the polarizability of the molecule and the electric field.

Therefore, $M = \alpha E_o \cos(2\pi \nu_o t)$.

The polarizability can be expressed as, $\alpha = \alpha_o + q\left(\frac{\partial \alpha}{\partial t}\right)_{q=0}$

Combining the above equations, the dipole moment M can be expressed as,

$$M = \alpha_o E_o \cos(2\pi \nu_o t) + q_o E_o \left(\frac{\partial \alpha}{\partial t}\right)_{q=0} [\cos(2\pi\{\nu_o - \nu_m\}t) + \cos(2\pi\{\nu_o + \nu_m\}t)]$$

In the above equation, the first term describes Rayleigh scattering, the second describes Stokes scattering, and the last describes Anti-stokes scattering.

Resonance Raman Spectroscopy

Resonance Raman Spectroscopy (RRS), a technique similar to Raman spectroscopy, is used to study the vibrational and rotational transitions of a molecule. In this technique, the excitation wavelength used is close to that required to cause an electronic excitation to the upper state (29). As a result, unlike Raman spectroscopy, RRS makes use of real electronic levels for scattering. Resonance Raman spectral band intensities are 10^7 times enhanced compared to the Raman spectral band intensities and can record the spectra of molecules present at very low concentrations. Figure 5 shows Raman and Resonance Raman transitions.

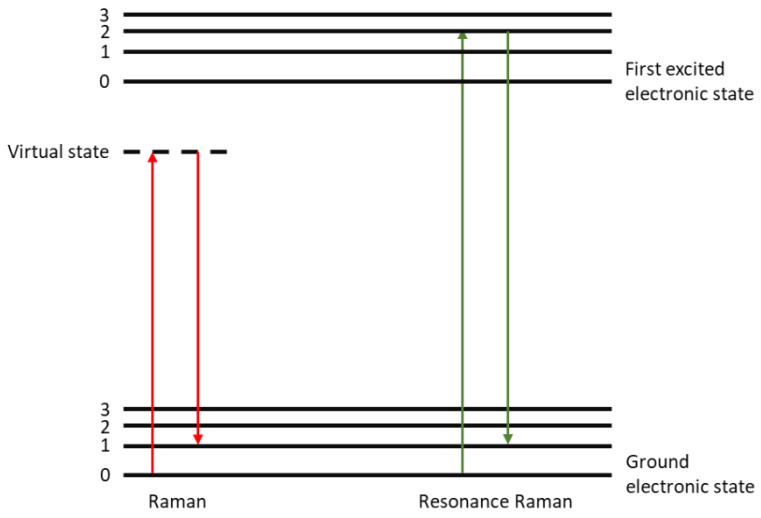

Figure 5. Schematic diagram of Raman and Resonance Raman scattering.

Photon Upconversion

When two or more long wavelength (low energy) photons are absorbed by an atom in a sequential manner, such that the absorption takes place through real excited electronic states, to emit a shorter wavelength (higher energy) photon, the process is called photon Upconversion. It is different from two-photon absorption because it takes place via real intermediate electronic states, in contrast to two-photon absorption which requires simultaneous absorption of two photons via virtual states. Moreover, photon upconversion through stepwise absorption has a higher absorption cross-section that two photon simultaneous absorption. Figure 6 shows an energy diagram for photon upconversion and two-photon absorption.

Photon upconversion was first proposed by Nicolaas Bloembergen in 1959 (30), and first observed experimentally by François Auzel in 1966 (31). Since then, many research activities have been focused on developing new upconverting micro and nanoparticles (32-34). Lanthanide based upconverting particles have gained the most attention because they are efficient and thus find unique applications in bioanalytical imaging (35-37), photovoltaic (38, 39), biosensing (40-42), and security (43) applications.

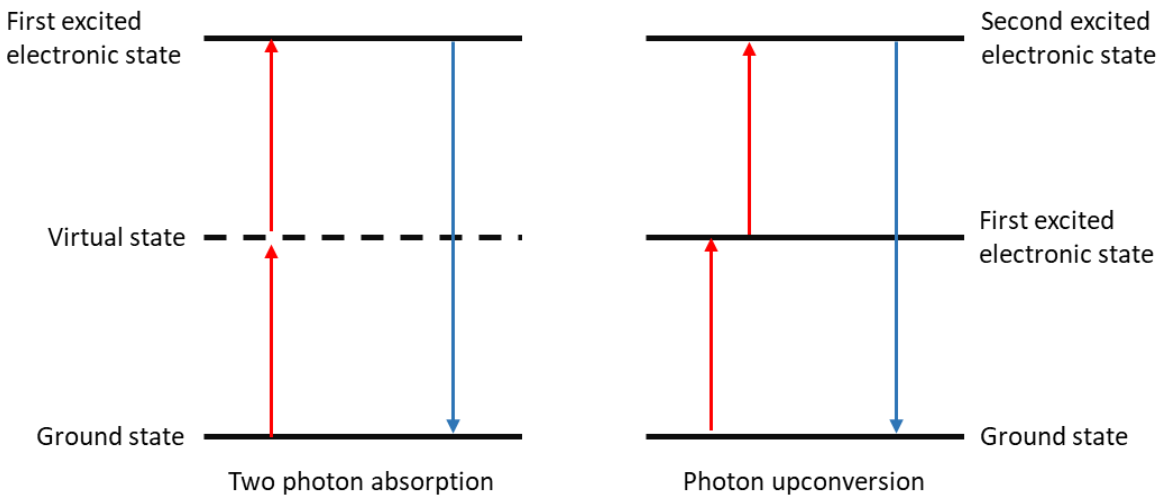

Figure 6. Two photon absorption and photon upconversion.

When lanthanide atoms are in the free state, 4f-4f transitions are forbidden (Laporte rule). However, when lanthanide ions are doped in a host lattice, these transitions become partially allowed due to the influence of the crystal potential that break the symmetry at the sites of lanthanide ions. This causes an abundance of equally-spaced electronic levels with long lifetimes. Moreover, the $5s^2 5p^6$ subshells shield the 4f electrons from the external surrounding (44) which results in a very narrow, line-like, emission band.

Most lanthanide-based upconverting particles consist of a stable dielectric host, doped with sensitizer and emitter ions. The sensitizer ions absorb incoming incident photons and transfer their energy to the activator ions. In our study, Yb^{3+} is used as the sensitizer owing to its large absorption cross-section of near-infrared light (NIR). These Yb^{3+} ions, and the Er^{3+} activator ions, are doped

in the $NaYF_4$ crystal lattice. This system is highly efficient in upconverting 980 nm NIR light to 540 nm green and 650 nm red light (45).

For lanthanide-doped upconverting particles, upconversion proceeds via three main mechanisms that include excited state absorption (ESA), energy transfer upconversion (ETU), and photon avalanche (PA). Figure 7 demonstrates these three mechanisms.

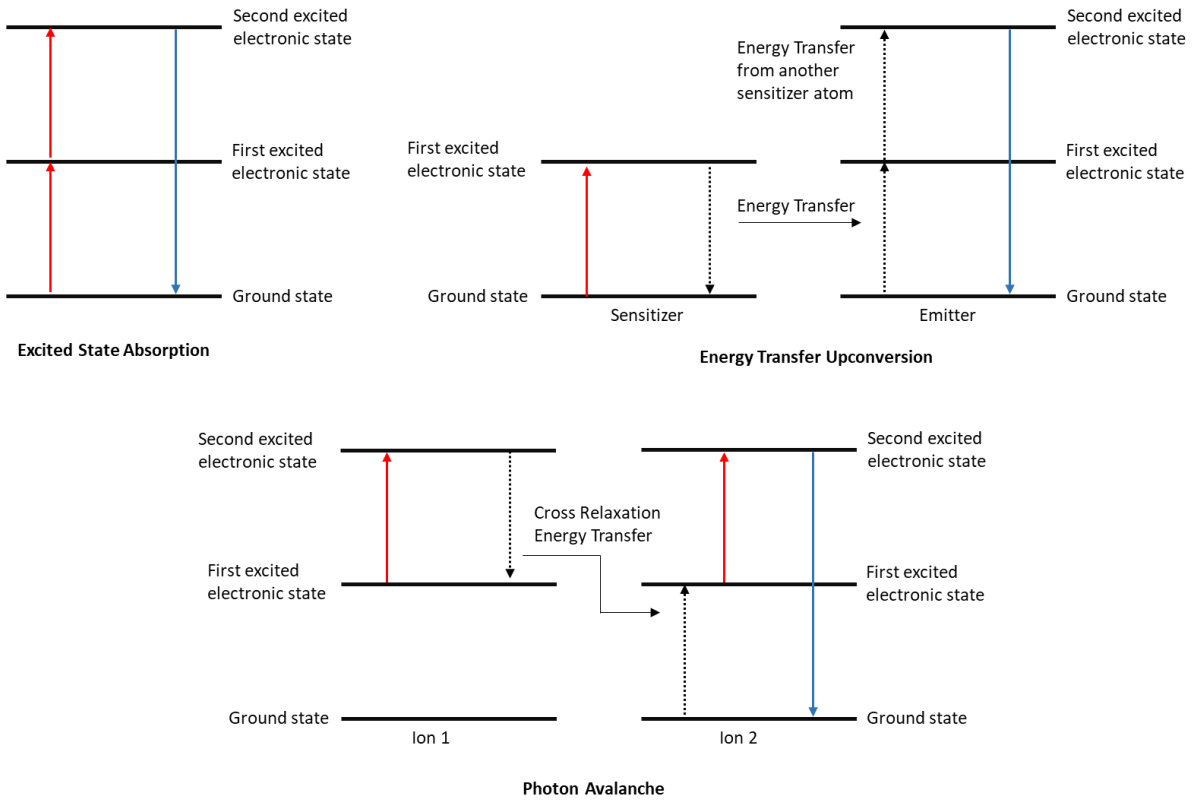

Figure 7. Mechanisms of photon upconversion: Excited State Absorption, Energy transfer Upconversion, and Photon Avalanche.

It is widely accepted that in the $NaYF_4$:Yb,Er system, the upconversion takes place through the ETU mechanism, in which the incoming photons excite the sensitizer ions to their excited states (45). The sensitizer ions transfer their energy to the activator ion which excites it from the ground state to higher excited states. This excited activator ion then relaxes to the ground state by emission of upconverted visible radiation. Figure 8 illustrates the ETU mechanism in $NaYF_4$:Yb,Er system.

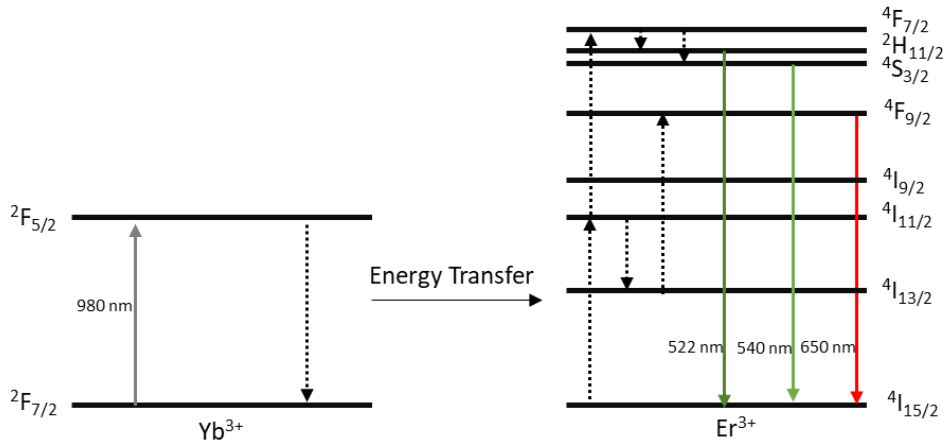

Figure 8. Energy Transfer Upconversion mechanism in $NaYF_4$:Yb, Er.

CHAPTER III

MATERIALS, METHODS, AND DEVICE DESIGN[*]

Detection of thymine dimers in thymine and DNA solutions

UV irradiation of thymine solution

Thymine, purchased from Sigma Aldrich, was used to prepare a 1.534 x 10^{-4} M aqueous thymine solution. 1 mL of this thymine solution was frozen at 240 K for 10 minutes and then irradiated with a mercury (argon) pencil lamp, which emits 0.66 mW/cm^2, 254 nm light. A bandpass UV filter, with a transmittance of 23.84% at 254 nm, was used to filter out wavelengths other than 254 nm. However, some proportion of 302 nm, 312 nm and 365 nm lines of the mercury pencil lamp were transmitted through the filter. This light was focussed onto the sample by a quartz lens and the thymine solution was irradiated for 5, 10, 20, 30, and 60 minutes. For each time irradiation interval, 1 mL was irradiated three times, in order to obtain a 3 mL irradiated solution, needed for measurements. Subsequently, the thymine was allowed to thaw for 10 minutes at 300 K before recording the absorption and Raman spectra.

UV irradiation of DNA Solution

Calf thymus DNA was purchased from Worthington Biochemical Corporation. 3 mL of aqueous DNA solution, 44.7 μm/mL, was irradiated at room temperature in a standard 10 mm path

[*] Parts of this chapter are reproduced from "Cell-phone camera Raman spectrometer" by D. Dhankhar et al., Rev. Sci. Instrum. 92, 054101 (2021), doi: 10.1063/5.0046281, with the permission of AIP Publishing; and " A novel approach for remote detection of bacteria using simple charge-coupled device cameras and telescope" by D. Dhankhar et al., Rev. Sci. Instrum. 91, 074106 (2020), doi:10.1063/5.0010701, with the permission of AIP Publishing; and "Resonance Raman Spectra for the In Situ Identification of Bacteria Strains and Their Inactivation Mechanism" by D. Dhankhar et al., Applied Spectroscopy (2021), doi:10.1177/0003702821992834, © 2021 Sage Publications; and "Thymine dissociation and dimer formation: A Raman and synchronous fluorescence spectroscopic study" by A. Nagpal et al., PNAS 118, e2025263118 (2021), doi: 10.1073/pnas.2025263118; and "Extending Human Vision to Infrared and Ultraviolet Light: A Study Using Micro-Particles and Fluorescent Molecules" by D. Dhankhar et al., IEEE Access 8, 73890-73897 (2020), doi:10.1109/ACCESS.2020.2988398.

length quartz cuvette. The irradiation was carried out using a mercury vapor lamp which emitted 3mW/cm^2 light. A UV filter was also used which transmitted 23.82% at 254 nm, allowing a band of 250 nm to 380 nm light to be transmitted. A quartz lens focused this light onto the aqueous DNA solution, which was irradiated for 30, 60, and 90 minutes.

Absorption and fluorescence spectra of thymine solution

The absorption spectrum of thymine solution was recorded by a Shimadzu UV160U spectrophotometer, with a spectral resolution fixed at 2 nm, for all absorption measurements. The fluorescence and synchronous fluorescence spectra were recorded using a Shimadzu RF-6000 fluorophotometer. The emission and excitation bandwidths were 3 nm. All spectra were recorded at room temperature in a 10 mm path length quartz cuvette, after each irradiation time interval.

Raman spectra of thymine solution

All Raman spectra were recorded using a Horiba XploRA PLUS Raman microscope. To record the spectra of thymine solution, a 5 μL drop was placed on a mirror and dried. The dried thymine was excited by a 532 nm laser in combination with a 10x objective lens and 1,200 grooves/mm grating. The Raman spectra of nonirradiated and irradiated thymine solutions, were recorded and corrected by choosing a common baseline, in order to remove the fluorescence background. All spectra were normalized to the 1,666 cm^{-1} spectral maximum, which arises due to C=O stretching in thymine. This was done in order to compare the Raman bands of all samples.

Raman spectra of DNA solution

The procedure for collecting the Raman spectra of DNA was similar to that used for thymine. A 20 μL drop of the DNA solution was placed on a mirror and dried. A higher volume was selected in order to easily identify the transparent DNA. A 638 nm laser, instead of 532 nm, was used for excitation in order to reduce the damage due to laser light, along with a 100x objective

lens and a 1,200 grooves/mm grating. All spectra were baseline corrected and normalized to the 1,335 cm^{-1} Raman band of adenine, whose intensity decreases very slightly upon UV irradiation.

Resonance Raman spectra of UV irradiated bacteria

Preparation of bacterial samples

The Micrococcus luteus bacteria were grown, at room temperature, on Tryptone Soya Agar (TSA) plates. The freshly grown bacteria were removed from the plates and suspended in a 12 mL saline solution. The bacteria were then centrifuged for 5 minutes, at 3300 rpm, using a Fisher Scientific 228 centrifuge. The supernatant was then removed, and the bacteria were again suspended in fresh saline solution. The process was repeated multiple times to remove the agar in the suspension. The concentration of the bacterial suspension was determined by its optical density (OD) at 600 nm, which represents the light scattering by the bacterial suspension. The OD at 600 nm was 0.5, which is equivalent to approximately 10^8 bacterial cells/mL.

UV irradiation of bacteria

3 mL of bacterial suspension, placed in a 10 mm path length quartz cuvette, was irradiated with 6mW/cm^2, 250 nm - 320 nm UV light, emitted by a mercury vapor lamp, while stirring continuously. The sample was centrifuged again, before recording its Raman spectra, in order to have a higher concentration of bacteria, about 10^{12} cells/mL, and achieve a higher signal to noise ratio. 10 μL of this concentrated bacteria suspension was placed on an aluminum mirror, and its Raman spectra were recorded.

Resonance Raman spectra of bacteria

A Horiba XploRA Raman spectrometer was used to record the resonance Raman intensities of bacterial samples using a 0.90 NA microscope objective. The excitation light, 532 nm, 25mW, was used to enhance the Raman signals due to the carotenoid pigments of the bacteria, as the absorption

bands due to this pigment lie between 450nm - 550nm. The resonance Raman spectra were recorded before and after 5, 10, and 20 minutes of UV irradiation. The spectra were baseline corrected and normalized with respect to the 1450 cm^{-1} lipid band, which shows minimal change on UV irradiation. The sample was visually monitored to check for signs of damage and two thermocouple sensors were also used to monitor the temperature at the laser focal spot.

The spectra were also recorded, before centrifugation, at a lower concentration, 10^8 cells/mL, using a 10x (0.25 NA) microscopic objective, in order to record spectra at different concentrations and hence determine the sensitivity of this technique.

Design of handheld instrument

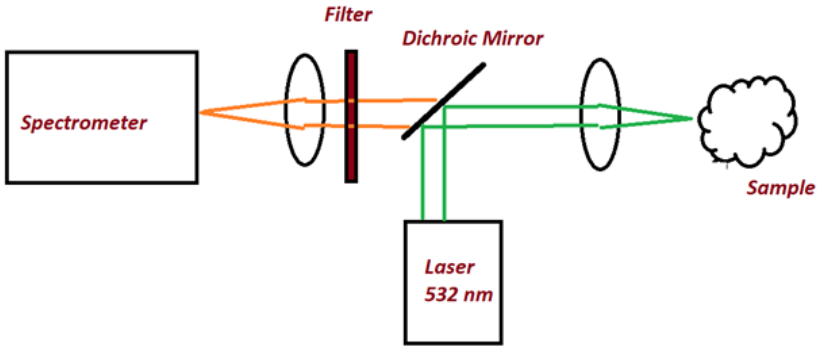

Figure 9. Schematic diagram of the resonance Raman handheld instrument. Reprinted with permission from (46).

Figure 9 shows a schematic diagram of the handheld instrument. This handheld device is based on backscattered, 180° geometry. It consists of a diode laser emitting 50 mW, 532 nm which was used as the excitation source, and a 0.25 NA microscope objective. A USB spectrometer with 1800 lines/mm diffraction grating and Sony ILX511B CCD were used for detection. The Raman spectrum of ethanol was used to calibrate the spectrometer. The dichroic mirror and Rayleigh rejection filter were obtained from Thorlabs.

Cell-phone Raman spectrometer

Device design

Traditional benchtop Raman spectroscopic instruments use the backscattered geometry for recording spectra, in which the direction of the laser light and axis of the collection lenses coincide with one another. Although this geometry results in very intense Raman bands, the excitation light is reflected back from the sample into the detector causing unwanted noise, in addition to noise due to Rayleigh scattering. In order to remove these sources of noise, dichroic mirrors and expensive Rayleigh rejection filters are used. These Rayleigh rejection filters can also reject the frequency region located less than 200 cm^{-1}.

In our instrument, we use a 90° geometry, wherein the direction of the laser light is perpendicular to the axis of the collection lens. This geometry reduces the intensity of Rayleigh scattering light reaching the detector, resulting in lower noise. In addition, this geometry allows for the analysis of bulk properties owing to the wide collection area of the lens. Fig 10 displays a schematic diagram of our cell-phone spectrometer.

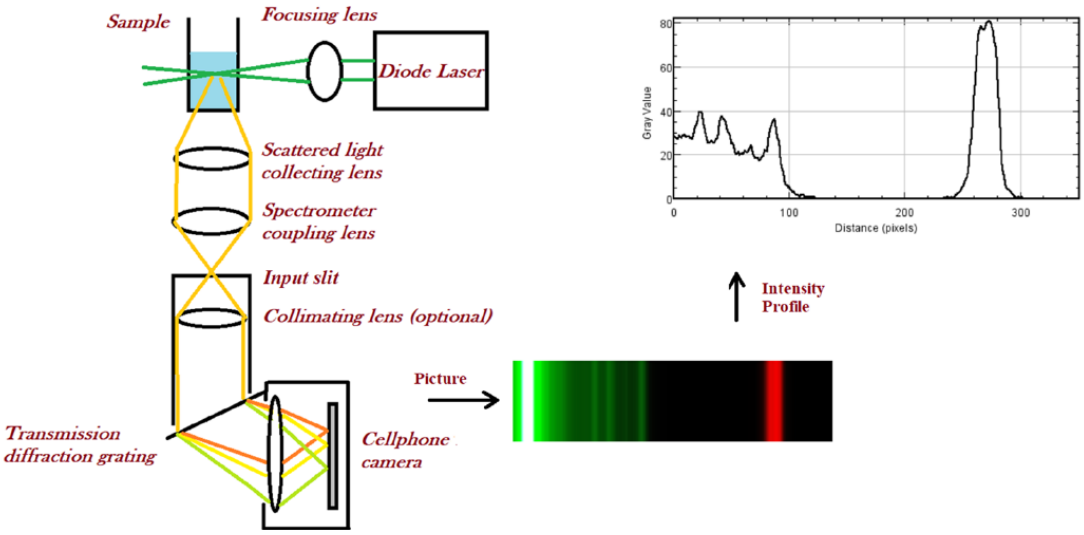

Figure 10. Schematic diagram of the Cell-phone Raman system. Reprinted with permission from (47).

A low-cost laser diode emitting 532 nm, 50 mW, light was used as the excitation source. A focusing lens, 10 mm focal length and 4 mm diameter, focused the light onto the sample. The Raman scattered light from the sample is collected by a two-lens system. The first lens collects and collimates the light from the sample, whereas the second lens focuses it, with a matching f-number, onto the spectrometer slit. Another collecting lens (25 mm diameter, 60 mm focal length), located inside the spectrometer, collimates the light onto a transmission grating (1000 lines/mm). The cell phone was placed behind the transmission grating. The spectra were acquired using a Google Pixel 3a (model XL) or Google pixel XL cell-phones. Figure 11 displays the top and the side views of this novel cell-phone Raman system.

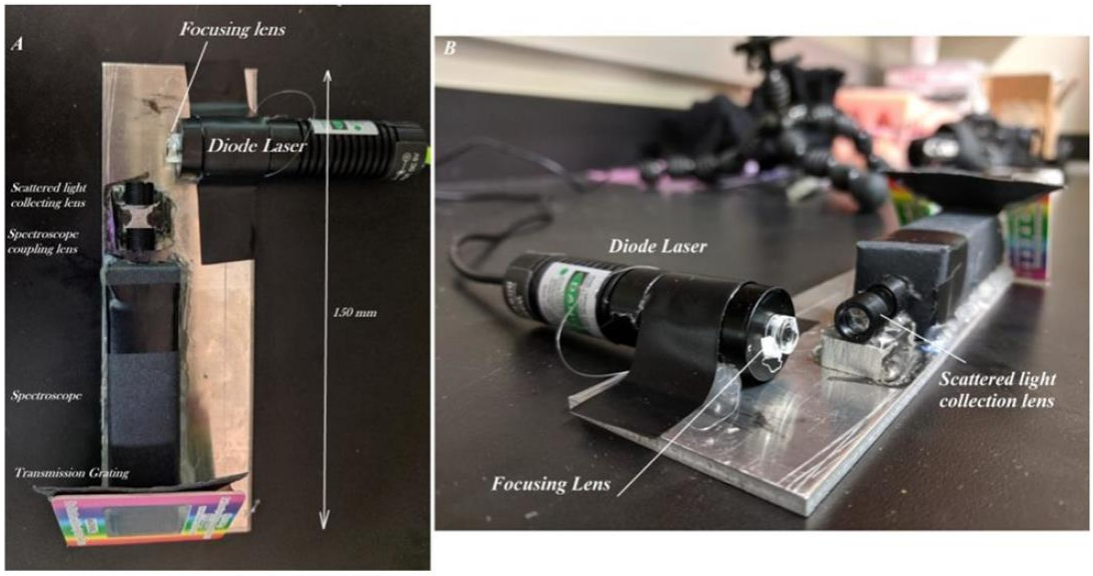

Figure 11. Top view (A) and side view (B) of the constructed cell-phone Raman device. Reprinted with permission from (47).

Acquisition of the Raman spectra

The spectra of various solvents including ethanol, methanol, isopropyl alcohol, and acetone were recorded in a 10 mm path length cuvette. Opaque samples such as carrots and bacterial pellets

were placed at the focal length of the focusing lens, at a 45° angle. For these samples, a Rayleigh line cut-off filter was employed.

The alignment was performed by recording the strong fluorescence spectrum of a solution of Rhodamine 6G. Then, Rhodamine 6G dye was replaced with the sample. The autofocus feature in the cell phone camera was used to focus onto the Rayleigh scattered light. These spectra were acquired in the night-sight mode, which provides an exposure time of up to 180 seconds, by averaging several small exposure times. In order to obtain a higher signal-to-noise ratio (SNR), other camera applications were used, such as HD Camera, which allowed for manual focusing, International Organization for Standardization (ISO) sensitivity, and exposure times of a few seconds. Multiple spectra were acquired and averaged in order to obtain high SNR. For example, 20 spectra were acquired and averaged when the exposure time was limited to 0.7 seconds.

For opaque samples, when Rayleigh line cut-off filters were used, the camera was focused onto the Rayleigh scattered light from a microparticle suspension. Subsequently, the microparticle suspension was replaced with the sample.

Image Processing

The recorded images were rotated, if needed, in order to display the vertical spectral lines. To remove noise from the spectrum, such as hot pixels, the vertical axis was binned by using the median value of all the pixels in that axis. The one-dimensional spectra were scaled in the vertical direction, and the spectral intensity was plotted against wavelength. The known Raman bands of ethanol were used to perform the pixel to Raman wavenumber calibration. Spectral rotating, binning, scaling, and intensity profile plots were all performed using the ImageJ software. Figure 12 shows the effect of spectral processing on the spectra of isopropanol, recorded by using the newly constructed system.

Figure 12. Raw (left) and processed (right) spectra of isopropanol in the fingerprint region. Reprinted with permission from (47).

The absorption spectrum of samples was recorded using a Shimadzu UV160 Spectrometer. The extraction of carotenes was performed using raw carrots in acetone solution. In order to determine the ethanol percentage in water solution, the HD camera app was used in the manual focusing mode, with 3.9 second acquisition time and ISO sensitivity of 7100.

Remote detection of bacteria using CCD camera and telescope

Device Design

The ratio of live and dead bacteria was determined by recording the change in fluorescence intensity of the bacteria, which is mainly due to tryptophan fluorescence, as shown previously by our group (5). We used the same technique, to develop a handheld instrument which, when used with a telescope, can remotely detect the ratio of live and dead bacteria, at a distance of several meters. This instrument uses a commercially available monochrome CCD, found in Closed Circuit Television (CCTV) cameras. These do not use Bayer filter, near-ultraviolet (NUV), and NIR filters, and therefore do not attenuate the UV light which is necessary for the detection of UV fluorescence from bacterial components. This device operates in two modes, the spectral collection mode and imaging mode, which are shown in Figure 13.

In the spectral collection mode, a fluorescence collection lens focuses the light onto the input slit of the spectrometer, such that the f-number of the collection lens matches that of the

spectrometer, therefore the entire area of the grating is illuminated. A homemade grating spectrometer was used, which consists of a 1000 lines/mm transmission diffraction grating, with a slit width of 0.5 mm. In the imaging mode, the visible light cutoff filter is placed in front of the camera to allow only the 330 nm – 380 nm fluorescence of tryptophan to pass through. The imaging data were collected using SharpCap in the video mode. 150 frames, acquired in 5 seconds, were averaged to obtain the final image. ImageJ software was used to obtain the spectral profiles and the fluorescence intensities from the final image. For both spectral detection and imaging modes, a 280 nm LED was used as the excitation source, with an output power of ~ 1mW. This light was collimated by a fused silica half-ball lens of 5 mm diameter.

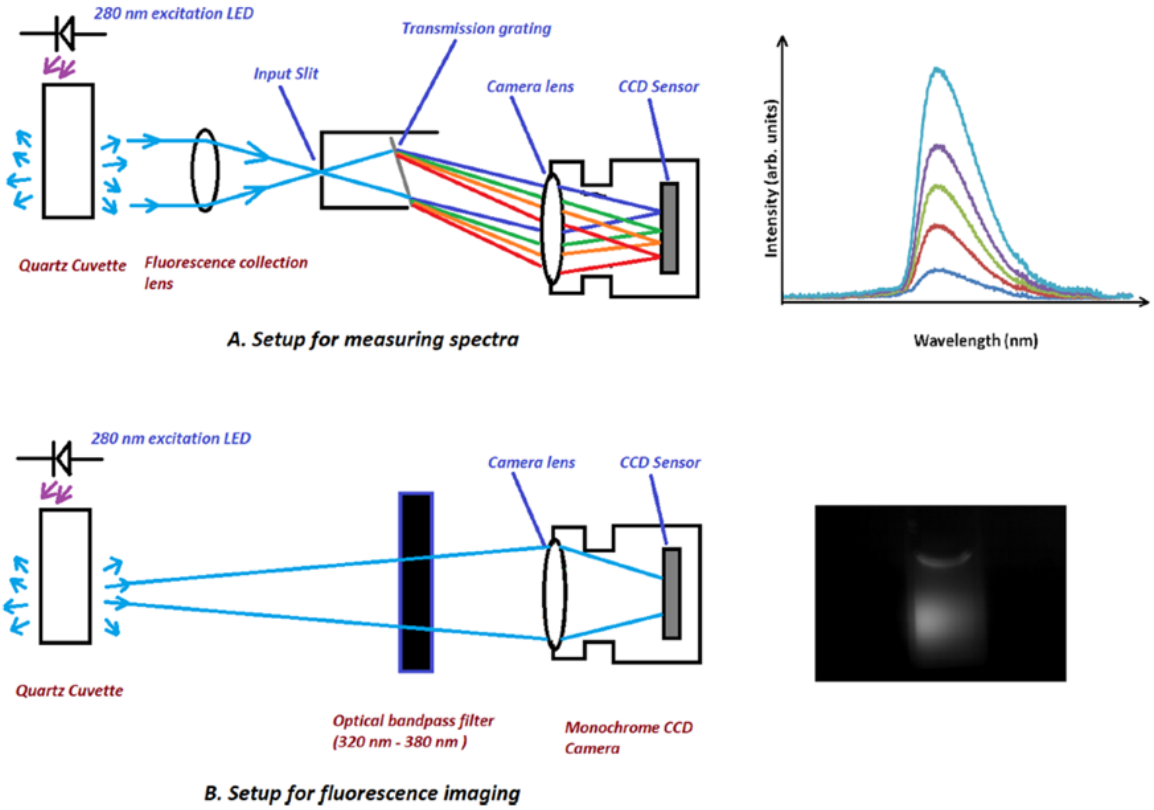

Figure 13. Experimental system used to record fluorescence spectra (A) and fluorescence image (B). Reprinted with permission from (48).

For remote detection from tens of meters away, the CCD camera was attached directly to the focuser of a telescope to achieve prime focus. For spectral collection, a fiber optic cable transmitted the light from the focus of the telescope to the input slit of the spectrometer. The excitation geometry was the same as in the previous cases, described above. Figure 14 displays the schematic diagram of our handheld instrument, which uses a telescope, for remote spectral collection and imaging of the fluorescence intensities emanating from different samples.

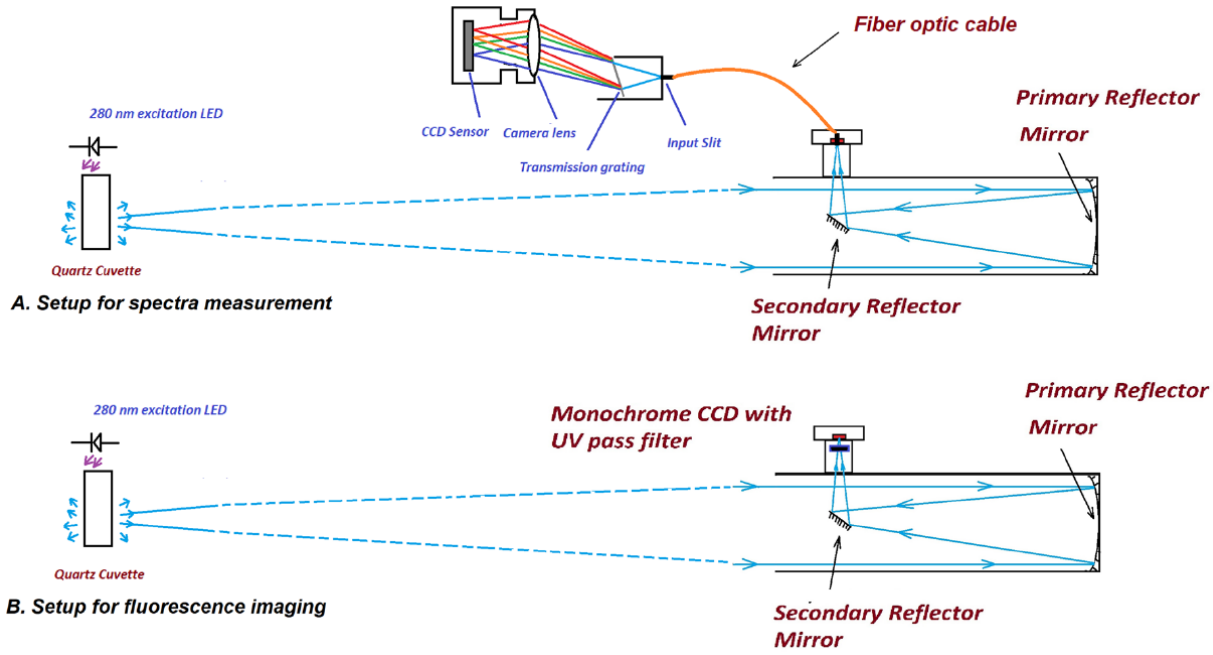

Figure 14. Schematic diagram of the telescope integrated with the handheld system for remote acquisiton of fluorescence spectra (A) and fluorescence images (B). Reprinted with permission from (48).

The same 280 nm LED was used to irradiate bacteria and record the spectra. The spectral acquisition time was 5 seconds, while the bacteria were irradiated for 5, 20, and 30 minutes. The UV irradiation power density on the sample was 0.5 mW/cm^2. 1.5 mL of bacterial sample was placed in a 10 mm path length cuvette and stirred continuously using a magnetic stirrer.

Preparation of bacterial samples

Escherichia coli (E. coli) bacteria were cultured on a TSA plate, subcultured in 10 mL Luria Bertani (LB) growth medium, and incubated overnight at 37° C. They were then harvested, in their stationary phase, by centrifugation at 3300 rpm for 5 minutes. The resulting pellets were mixed with saline solution and centrifugated, again. This procedure was performed three times in order to remove the growth medium. Then, a pellet was diluted in the saline solution, to a concentration of approximately 10^8 cells/mL. This was measured by recording the OD at 600 nm, and also by counting the Colony Forming Units (CFUs). The same procedure was performed for the growth and preparation of Bacillus thuringiensis bacteria.

Spectral and image processing

The spectral data recorded by the CCD camera was processed using SharpCap and further analyzed using the ImageJ software.

Extending vision to IR and UV regions

$NaYF_4$:Yb,Er microparticles, 1-5 μm in size, that convert IR to visible light, were purchased from Sigma Aldrich. Microparticles were used instead of nanoparticles because they exhibit higher IR to visible conversion quantum efficiency (49). Stilbene 420 dye, purchased from Exciton, was used, without further purification, to convert UV to visible light. This dye was selected because its emission spectrum overlaps with the absorption spectra of blue cones in the human eye and has a high fluorescence quantum yield. Green fluorescent protein (GFP), purchased from Sigma Aldrich, was also used to convert UV light to visible. The emission spectra of GFP overlaps with the absorption spectra of rod visual pigment.

The rod outer segments were mixed with the upconverting particles, stilbene-420 dye and a protein solution, for example, bovine serum albumin (BSA), egg albumin, etc. Another solution,

which consisted of GFP instead of stilbene 420, was also prepared. This was done to check if the upconversion efficiency changes in the proteins, which would pave way for their introduction in the eye without deleterious effects. The absorption and fluorescence spectra were recorded using Shimadzu UV-160U spectrometer and Shimadzu RF-5301PC spectrofluorophotometer, respectively.

Design of upconverting vision glasses

Figure 15 shows a schematic diagram of the vision glasses used to extend the human vision to near IR and near UV. The system consists of an objective lens, a screen coated with upconverting and fluorescent protein/dye, and an eyepiece lens. The screen is placed at the image plane of the objective lens. The upconverting particles, on the screen, will convert the infrared image, formed by the objective lens, to a visible image. The visible image formed at the focus of the eyepiece lens will then be projected to the eye.

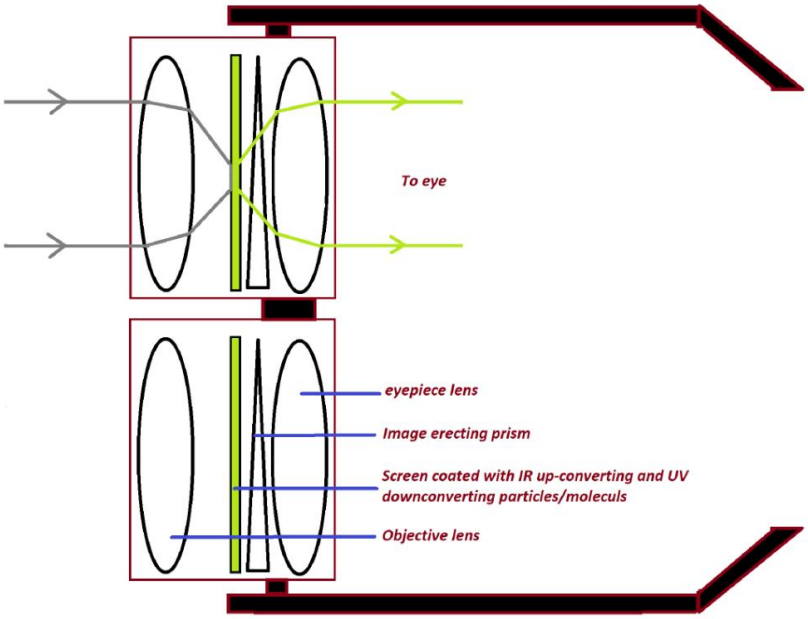

Figure 15. Schematic diagram of eyeglass device for extending vision in near infrared and near UV light. Reprinted with permission from (50).

CHAPTER IV

RESULTS AND DISCUSSION[†]

Detection of thymine dimers in thymine and DNA solutions

Raman spectra of non-irradiated and irradiated thymine solution

Figure 16 shows the Raman spectra of non-irradiated and irradiated aqueous thymine solutions. The maximum at 1665.71 cm^{-1} in the Raman spectrum of non-irradiated thymine solution is assigned to the C_4=O and C_5=C_6 stretching vibrations in the thymine monomer (51-53). When thymine is irradiated, this peak shifts toward 1686.62 cm^{-1} because the C_5=C_6 bond dissociates to form a single C-C bond with the adjacent thymine, forming a thymine dimer. As a result, the π electrons localize and strengthen the C_4=O bond, which consequently shifts to higher wavenumbers.

Figure 17 shows the change in the ratio of the thymine Raman intensities at 1686.62 cm^{-1} to 1665.71 cm^{-1} as a function of irradiation time, where the red dots represent the ratio of the intensities at 1686.62 cm^{-1} to 1665.71 cm^{-1} for each spectrum recorded, while the blue line represents the average of the aforementioned ratios for each irradiation time interval. It is clear, from this figure, that thymine converts to the dimer during the first 20 minutes of irradiation and

[†] Parts of this chapter are reproduced from "Cell-phone camera Raman spectrometer" by D. Dhankhar et al., Rev. Sci. Instrum. 92, 054101 (2021), doi: 10.1063/5.0046281, with the permission of AIP Publishing; and " A novel approach for remote detection of bacteria using simple charge-coupled device cameras and telescope" by D. Dhankhar et al., Rev. Sci. Instrum. 91, 074106 (2020), doi:10.1063/5.0010701, with the permission of AIP Publishing; and "Resonance Raman Spectra for the In Situ Identification of Bacteria Strains and Their Inactivation Mechanism" by D. Dhankhar et al., Applied Spectroscopy (2021), doi:10.1177/0003702821992834, © 2021 Sage Publications; and "Thymine dissociation and dimer formation: A Raman and synchronous fluorescence spectroscopic study" by A. Nagpal et al., PNAS 118, e2025263118 (2021), doi: 10.1073/pnas.2025263118; and "Extending Human Vision to Infrared and Ultraviolet Light: A Study Using Micro-Particles and Fluorescent Molecules" by D. Dhankhar et al., IEEE Access 8, 73890-73897 (2020), doi:10.1109/ACCESS.2020.2988398.

then remains constant, suggesting that the thymine dimer dissociates and converts back to the monomer(s). As a result, an equilibrium is established between the thymine dimers and monomers.

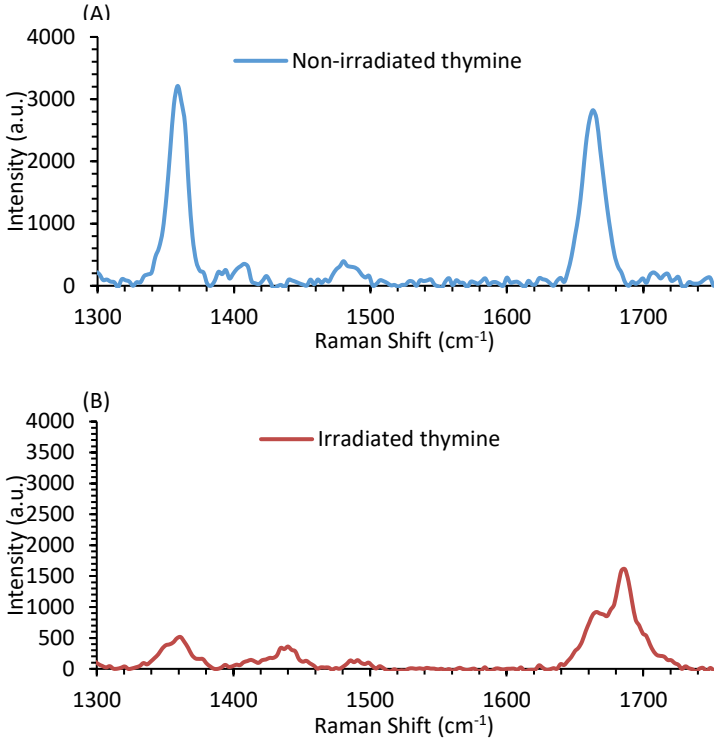

Figure 16. Baseline corrected Raman spectra, in the 1300 cm^{-1} to 1750 cm^{-1} region, of non-irradiated thymine (A), and irradiated thymine solution with 254 nm for 10 minutes (B). Reprinted with permission from (24).

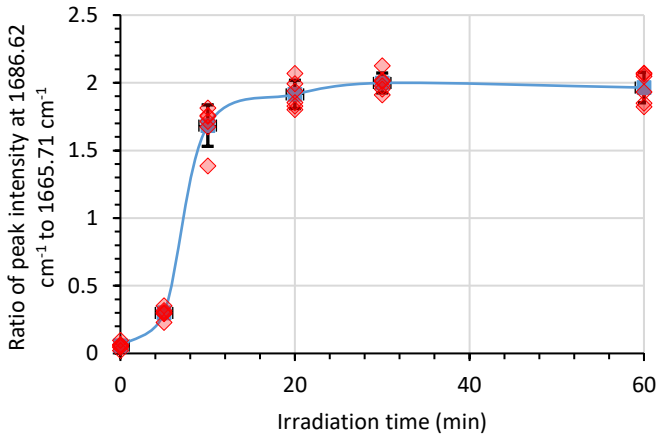

Figure 17. Change in the ratio of thymine Raman intensities at 1686.62 cm^{-1} to 1665.71 cm^{-1} as a function of irradiation time (min). Reprinted with permission from (24).

The maximum at 1361.41 cm^{-1} in the Raman spectrum of non-irradiated thymine solution is assigned to symmetric deformation (umbrella bending) of the CH_3 group connected with an sp^2 hybridized carbon atom (C_5 atom in this case) (51, 53). Figure 16 shows that as thymine is irradiated, the intensity of this band at 1361.41 cm^{-1} decreases because the C_5=C_6 bond dissociates to form a single bond. As a result, the CH_3 group bonded to C_5 atom is no longer bonded to an sp^2 hybridized carbon atom, but to an sp^3 hybridized carbon atom. The Raman scattering intensity of the bending frequency of the CH_3 group, bonded to an sp^3 carbon atom, is known to be very weak, and therefore it is, often, not observed by Raman spectroscopy. This occurs because the polarizability of the CH_3 group decreases owing to the loss of π electrons as the C_5=C_6 bond dissociates to form C_5-C_6.

Figure 18 shows the Raman spectra, of the non-irradiated and irradiated thymine solutions, recorded using the 100x objective. The maximum at 1246.26 cm^{-1}, assigned to the ring-stretching vibration of thymine, begins to decrease in intensity, after UV irradiation, and vanishes after 10 minutes of continuous irradiation. A similar decrease was also observed when DNA solution was irradiated, as discussed later in this paper.

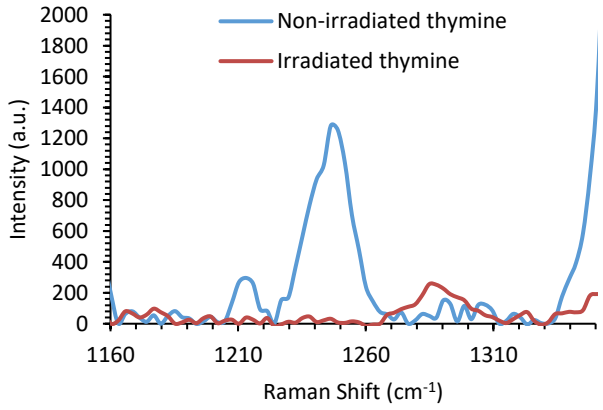

Figure 18. Decrease in the thymine Raman maxima at 1246.26 cm^{-1} on irradiation with 254 nm UV light. Reprinted with permission from (24).

Figure 19 shows the Raman spectrum of the non-irradiated and irradiated thymine solutions in the 2850 cm^{-1} to 3100 cm^{-1} region. It is observed that the thymine Raman band maximum at 3068.11 cm^{-1}, which is due to the C_6-H stretch when C_6 is sp^2 hybridized, vanishes on UV irradiation. When thymine monomers are irradiated, the C_5=C_6 bond dissociates to form a single C-C bond with another monomer. As a result, the C_6 atom becomes sp^3 hybridized, and causes the Raman maximum at 3068.11 cm^{-1} to shift below 3000 cm^{-1}. This occurs because as the bond strength decreases, the stretching frequency also decreases. We observed that upon UV irradiation, the maximum at 3068.11 cm^{-1} vanishes and a new broad band appears at 2986.4 cm^{-1}, which is a superimposition of several vibrational bands, as seen in Figure 19 (B).

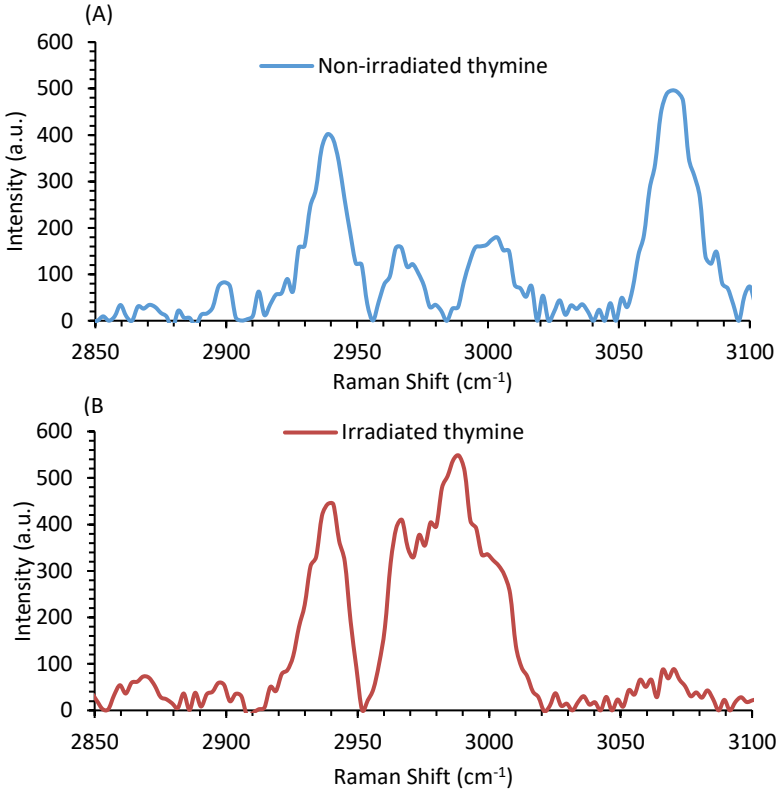

Figure 19. Baseline corrected Raman spectra, in 2850 cm^{-1} - 3100 cm^{-1} spectral region, of non-irradiated thymine solution (A), and thymine solution irradiated with 254 nm light for 10 minutes (B). Reprinted with permission from (24).

Raman spectra of non-irradiated and irradiated DNA solution

Figure 20 shows the Raman spectra of non-irradiated and irradiated DNA solutions. The maximum at 1375.36 cm^{-1} in the Raman spectra of the unirradiated DNA solution is assigned to the vibrational bands of Thymine, Guanine, and Cytosine. A decrease in this maximum is observed when DNA is irradiated with UV light which is similar to the decrease observed in the 1361.41 cm^{-1} maximum of the thymine non-irradiated and irradiated solutions. Therefore, we conclude that this decrease is attributed to the dissociation of the thymine base, as the UV irradiation-induced purine photoproducts are found to be several orders of magnitude smaller than the thymine photoproducts (23, 54).

The maximum at 1247.79 cm^{-1} in the Raman spectra of non-irradiated DNA solution, displayed in Figure 20, is assigned to the vibrational band of Thymine (55, 56). The same band occurs in the non-irradiated solution of thymine, at 1246.26 cm^{-1}, which is attributed to the ring stretching vibration of thymine. In both thymine and DNA, this maximum decreases on UV irradiation due to the formation of photoproducts. Similarly, the broad band at 1665.35 cm^{-1} in the Raman spectra of non-irradiated DNA, shown in Figure 20, is due to the superimposition of Raman bands of Thymine, Cytosine and Guanine (55). We observed a decrease in this Raman band, which is similar to that seen in the Raman spectrum of thymine solution after UV irradiation.

It is important to note that the changes in the Raman spectra of non-irradiated and irradiated DNA solutions, display similar changes to those observed in the Raman spectrum of non-irradiated and irradiated thymine solutions. Therefore, we have shown, for the first time, that the formation of thymine photoproducts in DNA can be observed spectroscopically by Raman analysis.

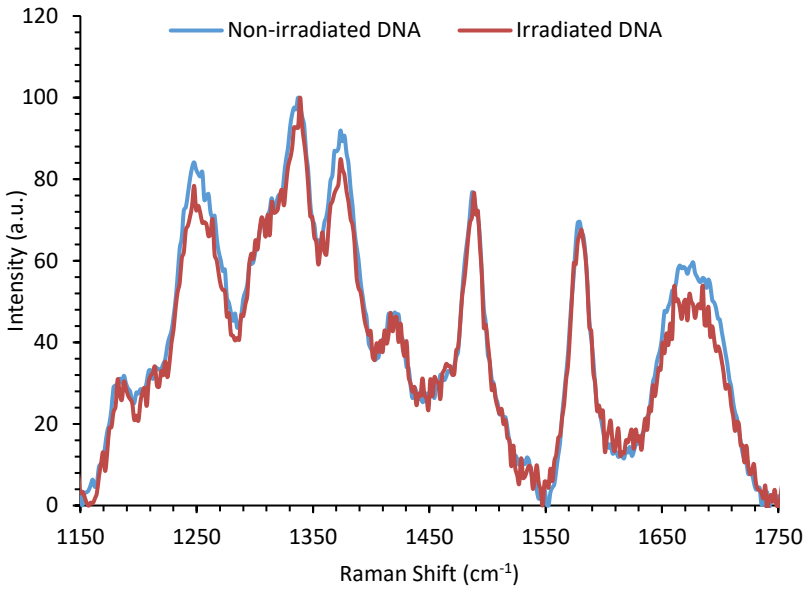

Figure 20. Normalized Raman Spectra of non-irradiated DNA (blue) and DNA irradiated for 30 minutes with 254 nm UV light (red). Reprinted with permission from (24).

Resonance Raman spectroscopy of UV irradiated bacteria

Effect of UV light on bacterial pigments

Figure 21 shows the resonance Raman spectra of Micrococcus luteus bacteria excited with 532 nm laser light. Since the wavelength of the laser light is close to the absorption peak of the carotenoid pigment (Sarcinaxanthin) present in bacteria, the Raman bands arising due to this pigment become prominent in the resonance Raman spectra. The Raman band at 1525 cm^{-1} is assigned to the carotenoid pigment's C=C stretching vibration, whereas the band at 1155 cm^{-1} is assigned to the C-C stretching vibrations (57-59). The intense band at 1002 cm^{-1} is assigned to the C-C-CH_3 bond deformation in the pigment (57). Less intense vibrational maxima at 1580 cm^{-1}, 1124 cm^{-1}, and 745 cm^{-1} are also assigned to the carotenoid pigment's vibrations. The bands at 1650 cm^{-1} and 1450 cm^{-1} are assigned to Amide I polypeptide vibrations and lipid H-C-H deformations (60-62).

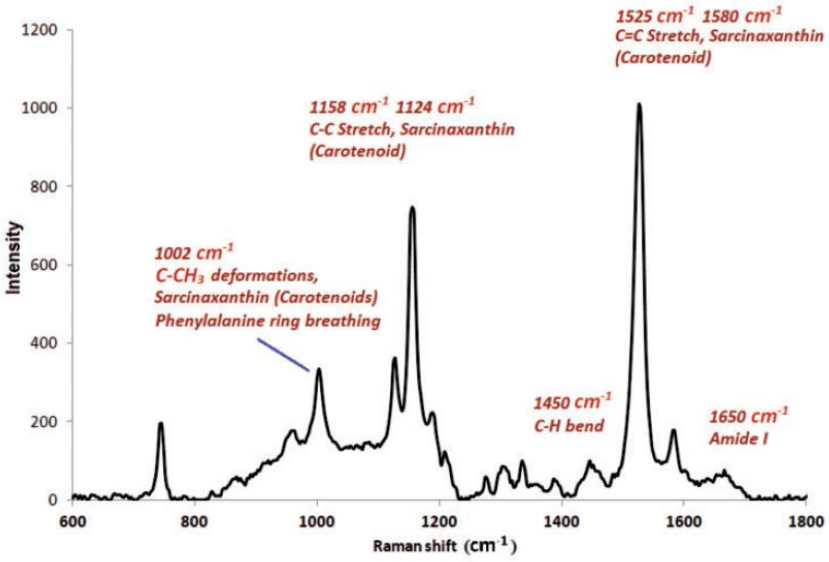

Figure 21. Resonance Raman spectrum of Micrococcus luteus bacteria excited with 532 nm laser light. Reprinted with permission from (46).

Figure 22 depicts the resonance Raman spectra of non-irradiated and irradiated Micrococcus luteus bacteria. The fluorescence background in these spectra was first removed and then the spectra were normalized with respect to the 1450 cm^{-1} band. It is observed that, upon UV irradiation, the Raman bands at 1525 cm^{-1}, 1158 cm^{-1}, 1127 cm^{-1}, 1007 cm^{-1}, and 1193 cm^{-1}, corresponding to the carotenoid pigment, decrease as a function of irradiation dose. We also observed a small, broad band, increase at 1400 cm^{-1} as a function of UV irradiation, similar to that observed in our studies with Escherichia coli bacteria (63). This increase was observed in several experiments and with different baseline fits. We have previously assigned this increase to the formation of UV induced protein photoproducts because pure proteins, on irradiation with UV light, also show a similar increase in this wavenumber region (63).

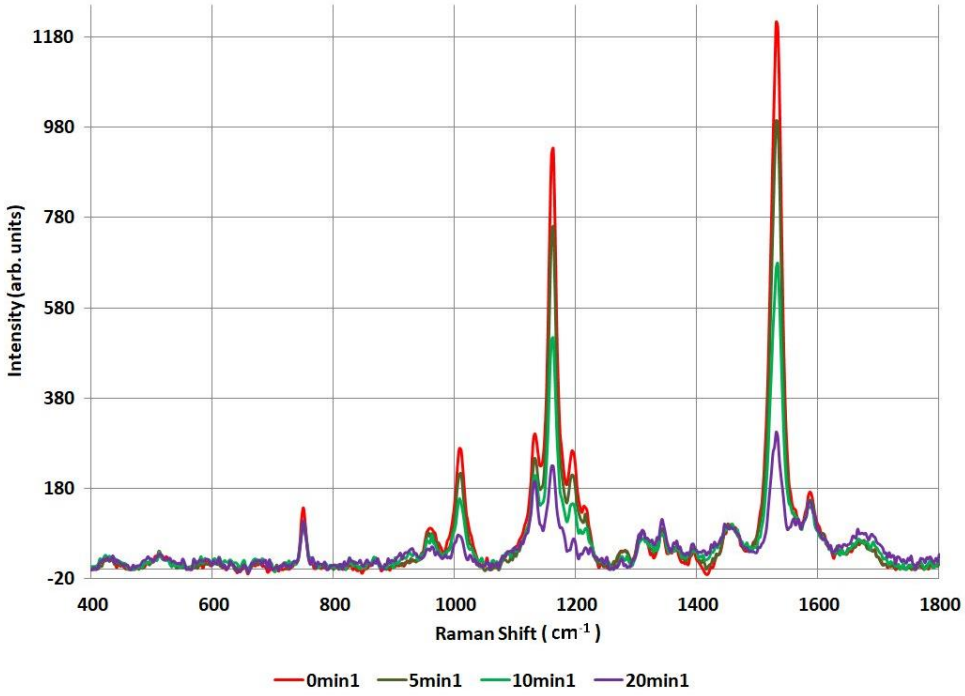

Figure 22. Resonance Raman spectra of Micrococcus luteus bacteria irradiated with UV light. Reprinted with permission from (46).

The ratio of Raman intensities at 1525 cm^{-1} to 1450 cm^{-1} and 1158 cm^{-1} to 1450 cm^{-1}, as a function of irradiation dose, is displayed in Figure 23 (A) and (B), respectively. We observe a strong decrease in the intensity of the Raman bands corresponding to carotenoid pigment's vibrations due to the bleaching of this pigment on UV irradiation, as these pigments also absorb UV light. The changes in the Raman bands can be used as spectroscopic signatures of inactivated bacteria which can be further used to quantify the UV irradiation effects on bacteria. Although the reduction in the Raman bands cannot be used as definite markers for inactivated bacteria, they can be used to correlate with inactivated bacteria and to estimate the ratio of live and dead bacteria. We found that after irradiating the bacteria for 5 minutes, the ratio of 1525 cm^{-1} to 1450 cm^{-1} Raman intensities decrease from 12.1 to 10.2. Upon plating and counting the Colony Forming

Units (CFUs) of these bacteria, we observe that the live bacteria population decrease by 4 to 5 orders of magnitude.

Previous studies have shown that the carotenoid pigments in bacteria may also undergo bleaching under intense laser irradiation (59, 64). In this study, we have ascertained that our laser light does not induce any damage to the bacteria.

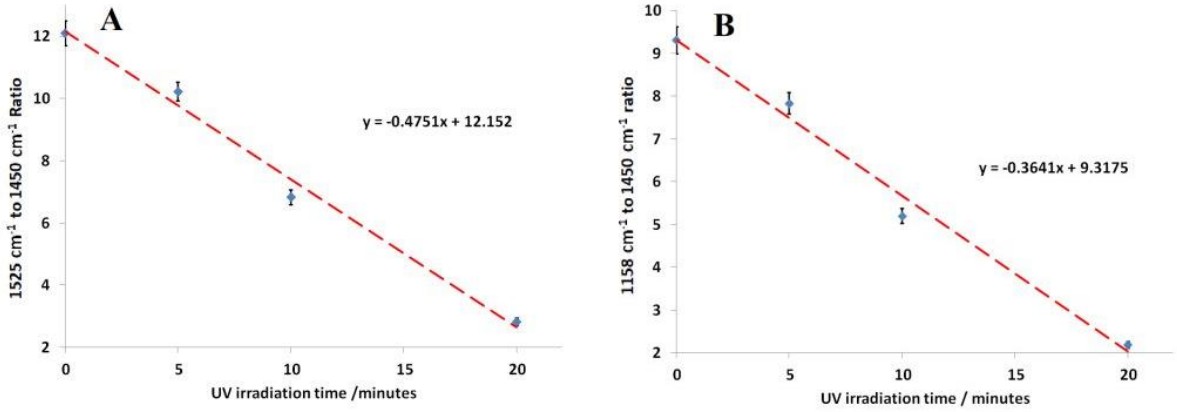

Figure 23. Ratio of Raman intensities at 1525 cm^{-1} to 1450 cm^{-1} (A), and 1158 cm^{-1} to 1450 cm^{-1} (B), as a function of irradiation dose. Reprinted with permission from (46).

Identification of bacterial strains

Although different bacterial strains contain similar carotenoid pigments, we can use this technique to differentiate between bacteria. This is because the length of the pigment polyene chain, such as carotenoid, can cause a change in the wavenumber of different vibrations (59). Moreover, some carotenoids may display unique bands in the Raman spectra due to different molecules bonded at the chain end. Figure 24 (A) shows the Raman spectra of M. luteus, E. coli, and S. marcescens. E. coli bacteria do not contain any pigment, and hence they do not exhibit Raman bands due to carotenoids. The spectra of S. marcescens and M. luteus both show prominent carotenoid bands, but also exhibit their unique spectral features which are used to identify

pigmented bacterial strains. We have used Principle Component Analysis (PCA) to differentiate between different bacterial strains, as shown in Figure 24 (B).

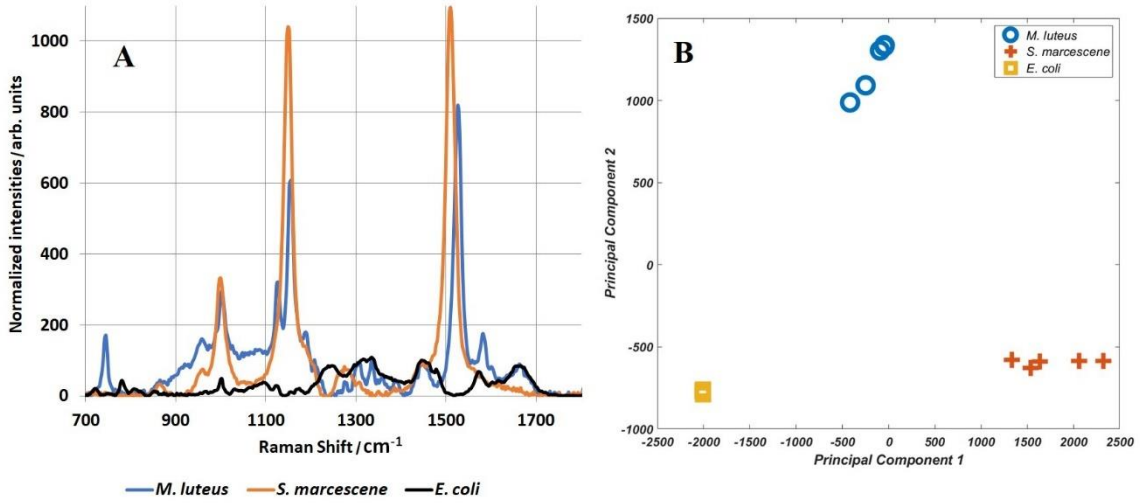

Figure 24. Raman spectra of M. luteus, E. coli, and S. marcescens (A) and Principle Component Analysis plot (B) for the identification of different bacterial strains. Reprinted with permission from (46).

Hand-held resonance Raman instrument

Figure 25 shows the resonance Raman spectrum of S. marcescens bacteria, recorded by the handheld instrument. After the baseline of the spectrum was removed, the spectral resolution was measured to be about 35 cm^{-1}, which is sufficient for the detection and identification of bacterial strains.

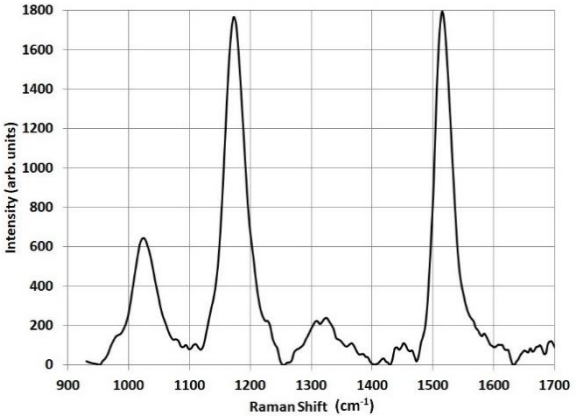

Figure 25. Resonance Raman spectrum of S. marcescens bacteria recorded by the handheld instrument. Reprinted with permission from (46).

Cell-phone Raman Instrument

Spectral Resolution

The Raman spectrum of ethanol, shown in Figure 26, was recorded using the cell-phone Raman instrument. The spectral resolution of the instrument was calculated by fitting the 885 cm^{-1} band maximum of ethanol to a gaussian curve. The FWHM = $2\sigma\sqrt{2ln2}$, where σ is the standard deviation, was thus calculated to be 49.47 cm^{-1}.

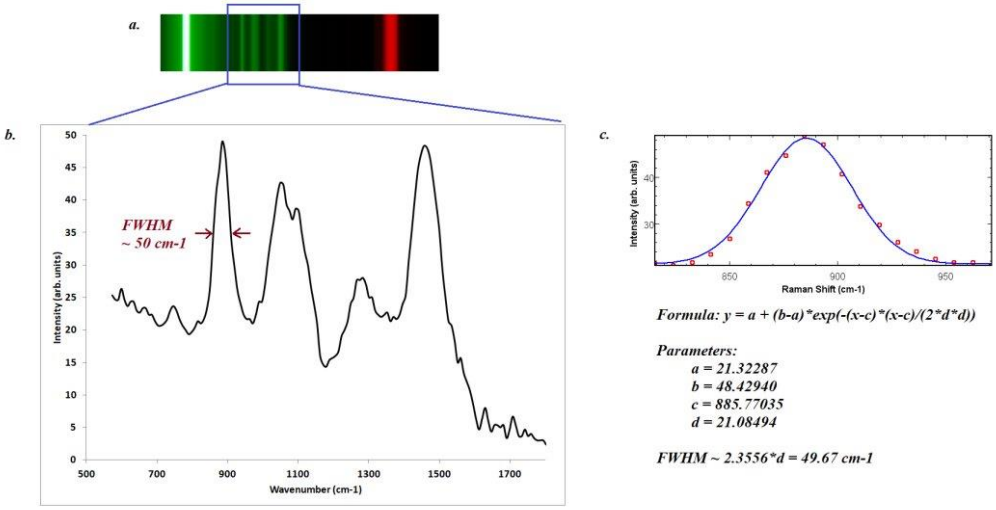

Figure 26. Spectral resolution of the cell-phone Raman instrument. Reprinted with permission from (47).

Recording the Raman spectra of various samples

Figure 27 displays the processed Raman spectra of ethanol, methanol, and isopropyl alcohol recorded using the cell-phone Raman instrument, and their corresponding intensity plots.

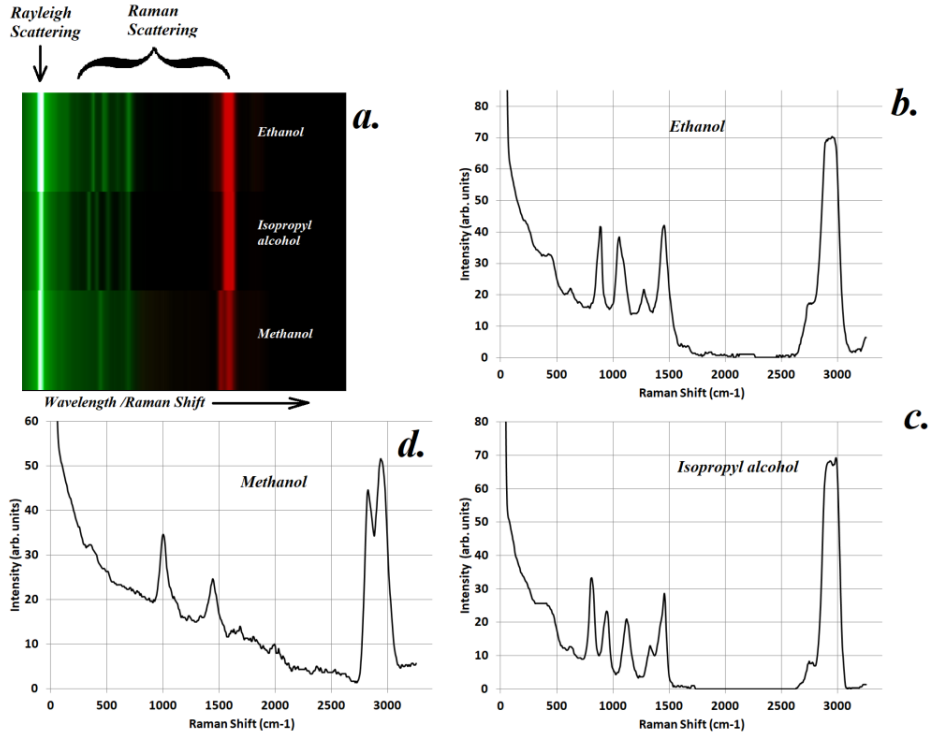

Figure 27. Processed Raman spectra of ethanol, methanol, and isopropyl alcohol and their corresponding intensity plots. Reprinted with permission from (47).

Figure 28 shows the resonance Raman spectrum of carrots, wherein the Raman bands due to the carotene pigments are enhanced because the electronic absorption transition is close to the 532 nm laser wavelength.

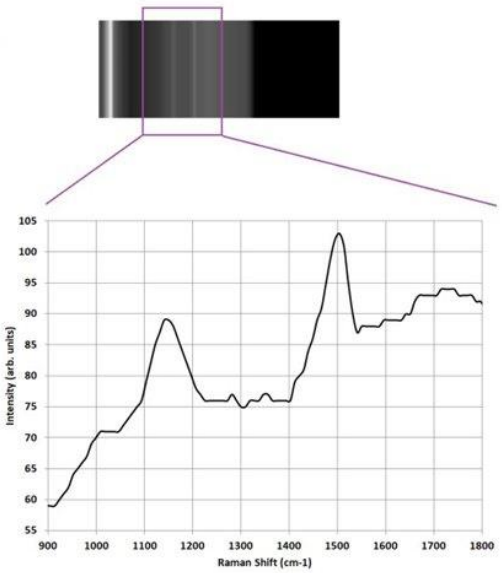

Figure 28. Raman spectrum of carrots (top) and corresponding intensity plot (bottom). Reprinted with permission from (47).

Quantitative Analysis

In order to test the accuracy of this instrument for quantitative analysis, we calculated the ratio of ethanol's 2935 cm^{-1} Raman maximum to that of water's 3400 cm^{-1} Raman maximum, at several, known concentrations of ethanol-water solutions, as shown in Figure 29. Such analysis is useful for the determination of the ratio of active ingredients in consumer products.

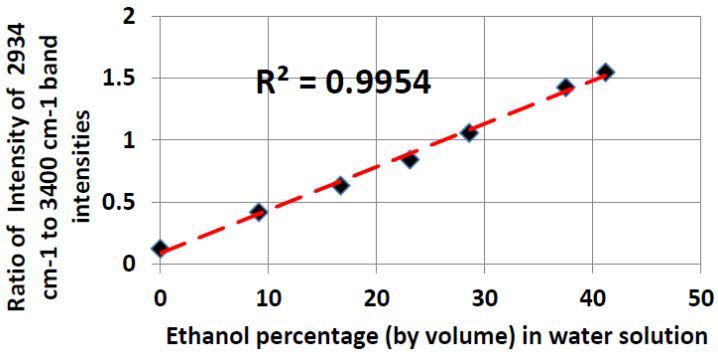

Figure 29. Ratio of intensity at ethanol's 2935 cm^{-1} to water's 3400 cm^{-1} maximum as a function of ethanol-water solution concentration. Reprinted with permission from (47).

Recording 2-D Raman Spectral Images

This instrument can also be used for recording 2-D spectral images by scanning the sample in both vertical and horizontal directions. We recorded the Raman spectra of water and ethanol samples, in two different cuvettes. It can be seen in Figure 30, the water's red colour is due to the intensity of the 3400 cm^{-1} Raman band, whereas ethanol's green colour corresponds to ethanol's 2935 cm^{-1} Raman band.

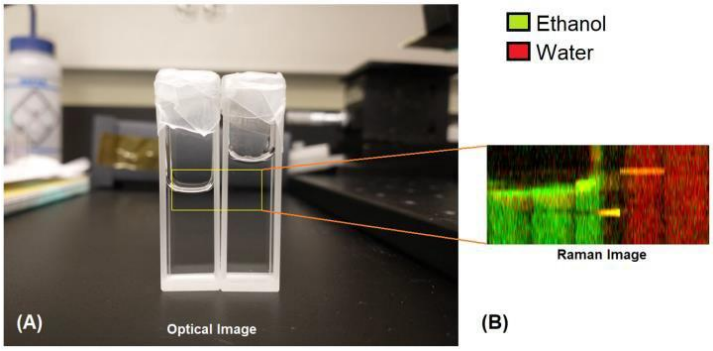

Figure 30. Image of the two cuvettes containing ethanol and water samples (A) and Raman image of the scanned region (B). Reprinted with permission from (47).

Comparison of the cell-phone Raman instrument with conventional Raman instrument

The cell-phone Raman instrument was compared to a very sensitive benchtop Raman system, HORIBA XploRA PLUS. Using distilled water as the test sample, we measured the Signal to Noise Ratio (SNR) of the recorded Raman spectra from the two systems. Figure 31 shows the Raman spectra of water recorded by these two instruments with an excitation numerical aperture (NA) of nearly 0.25 for both instruments. As seen in the figure, for the benchtop HORIBA system, the SNR is one order of magnitude higher than our constructed cell phone system. It was also observed that the SNR of our constructed instrument improves by a factor of 2 when we used only the red channel instead of using all RGB channels. This is because most signal falls in the red

channel while the other channels contribute to noise in the signal. The noise in the cell phone system is also attributed to the CCD/CMOS sensors used in the cell phone cameras compared to the specialized CCD detectors used in the benchtop systems. Uncooled detectors, small pixel sizes, and lower diffraction efficiency of the grating used in our system could be other factors contributing to lower SNR.

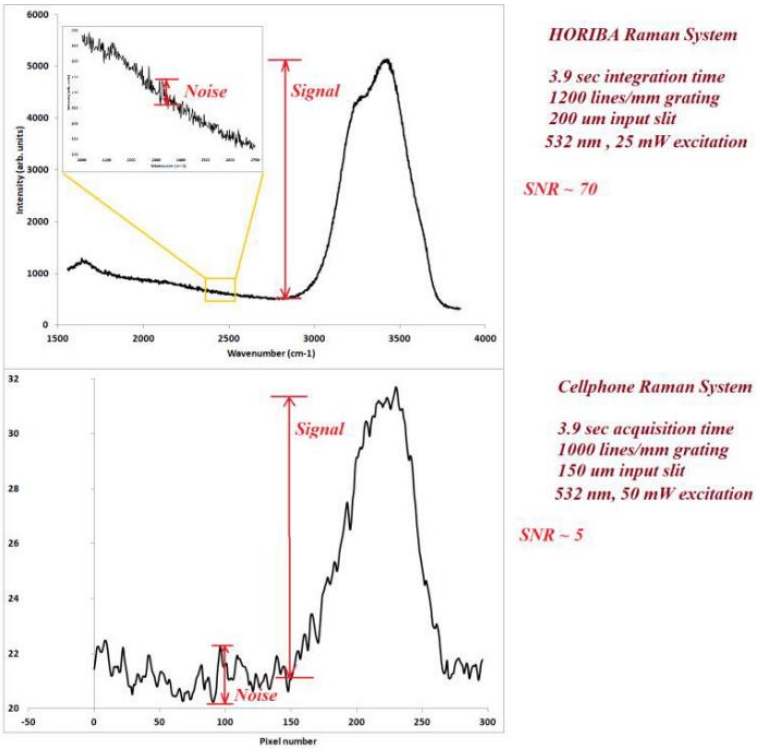

Figure 31. Comparison of SNR of Raman spectra of water recorded using benchtop Raman system and the cell-phone Raman instrument. Reprinted with permission from (47).

Remote detection of pathogens using CCD camera and telescope

Figure 32 displays the fluorescence spectra of tryptophan at various concentrations, recorded by the transmission grating monochrome camera. The lowest concentration of tryptophan that could be detected was less than 200 ng/mL.

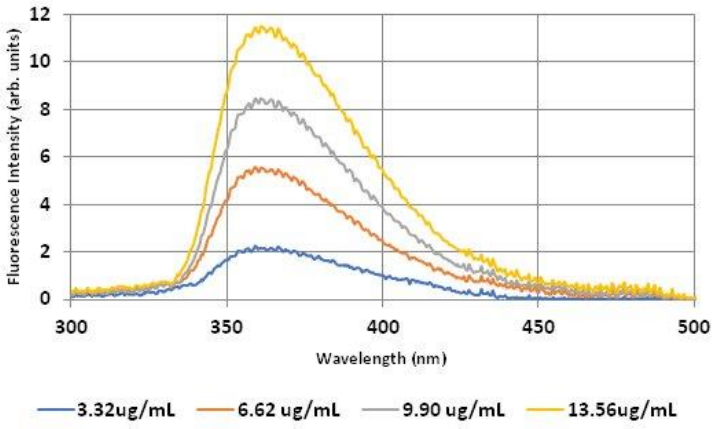

Figure 32. Fluorescence spectra of tryptophan, at various concentrations, recorded by the CCD camera-spectrometer system. Reprinted with permission from (48).

We have previously reported (5) that as the ratio of live and dead bacteria decreases, due to UV exposure, the tryptophan fluorescence intensity also decreases. Figure 33 (A) shows the fluorescence spectra of E. coli bacteria as a function of UV dose, while Figure 33 (B) is a plot of the number of E. coli bacterial colonies before and after irradiation vs the fluorescence intensity at 350 nm attributed to tryptophan fluorescence.

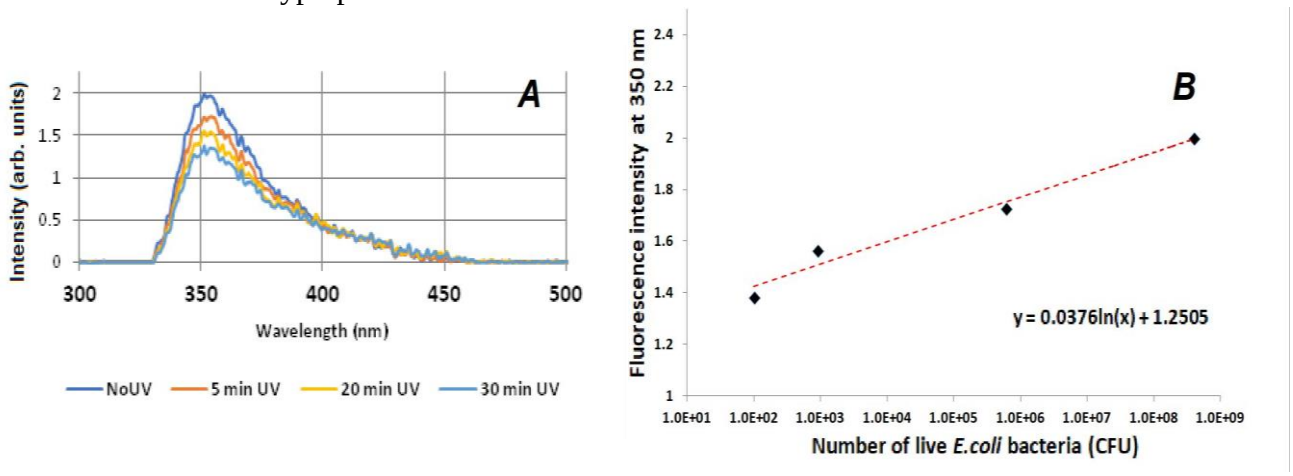

Figure 33. Fluorescence spectra of E. coli as a function of UV dose (A), E. coli colonies counted, before and after irradiation, vs fluorescence intensity at 350 nm (B). Reprinted with permission from (48).

Remote detection of bacterial tryptophan fluorescence

Figure 34 displays the fluorescence spectrum of tryptophan, recorded at 10 m from the sample, using our spectrometer with the telescope.

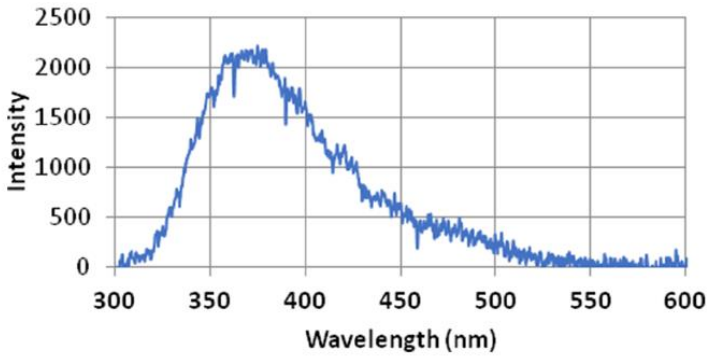

Figure 34. Fluorescence spectrum of tryptophan, recorded at 10 m from the sample, using the constructed spectrometer with a telescope. Reprinted with permission from (48).

Extending vision to IR and UV regimes

Upconverting particles dispersed in proteins

The upconverting particles were dispersed in proteins, including bovine serum albumin (BSA), egg albumin, whey (milk) protein, and green fluorescent protein (GFP), in order to check their upconversion efficiency in different proteins, which provide the advantage of their possible insertion into the eye. Figure 35 shows the upconversion behaviour of these microparticles in different proteins.

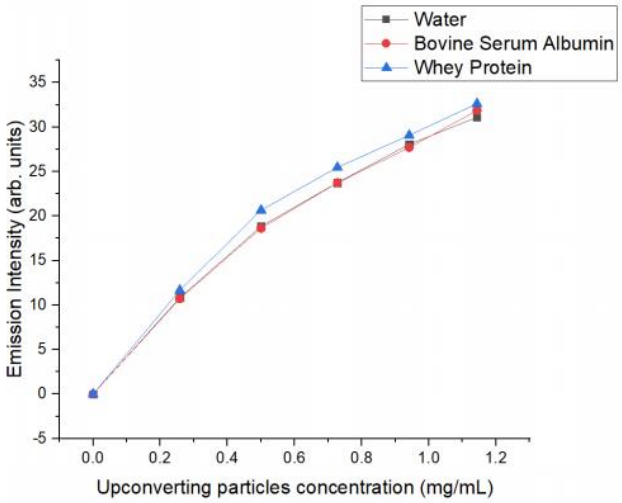

Figure 35. Intensity of upconverted light vs concentration of microparticles in water, BSA and whey protein. Reprinted with permission from (50).

Stilbene-420 dye dispersed in proteins

In order to convert UV light to visible, we use Stilbene-420 dye which emits 425 nm blue fluorescence light on excitation with UV light (330 nm – 380 nm). When mixed with different proteins, including BSA, whey protein, and egg albumin, it is found that no fluorescence quenching is observed for egg albumin and whey protein. However, in BSA, the fluorescence intensity decreases by a factor of 4-5.

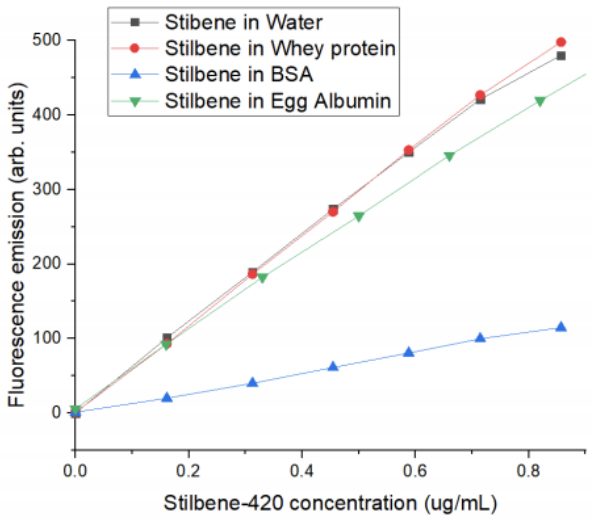

Figure 36. Fluorescence intensity of Silbene-420 dye as a function of concentration in water and various proteins. Reprinted with permission from (50).

Although Stilbene-420 dye can efficiently convert UV to visible light, it cannot be used inside the eye, at the retina. This is because Stilbene-420 has an absorption maximum at 350 nm, which is strongly attenuated by the human eye lens and tissues. Therefore, it can only be used inside wearable eyeglasses outside the eye. An alternative to Stilbene-420 is GFP. GFP has an absorption maximum at 390 nm and its fluorescence overlaps with the absorption spectrum of mammalian rod visual pigment.

Combining upconverting particles with Stilbene-420/GFP

We observed that on the addition of upconverting particles to fluorescent proteins (Stilbene-ovalbumin mixture, GFP), both retained their spectroscopic properties. Figure 37 shows the fluorescence emission of GFP and emission of upconverting particles when excited by 395 nm UV and 980 nm IR light, respectively. Figure 38 displays the fluorescence emission of Stilbene-420 dye mixed with ovalbumin and emission of upconverting particles when excited by 360 nm UV and 980 nm IR light, respectively.

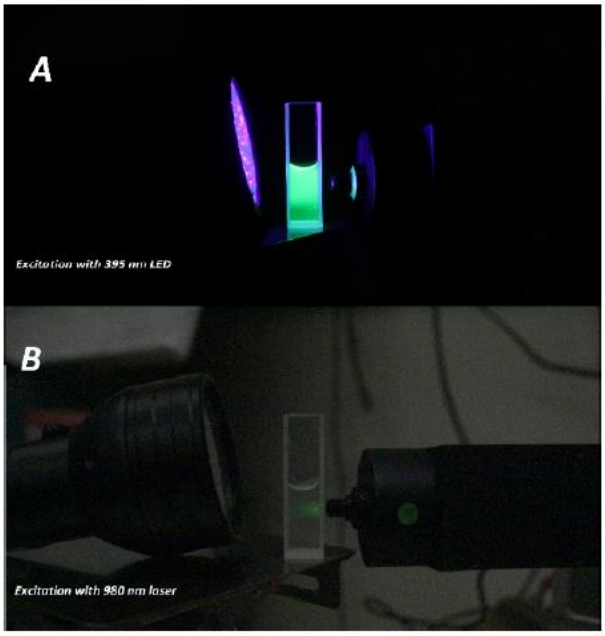

Figure 37. Fluorescence emission from GFP under 395 nm UV excitation (A), Upconverted light emission from upconverting microparticles excited by 980 nm IR light (B). Reprinted with permission from (50).

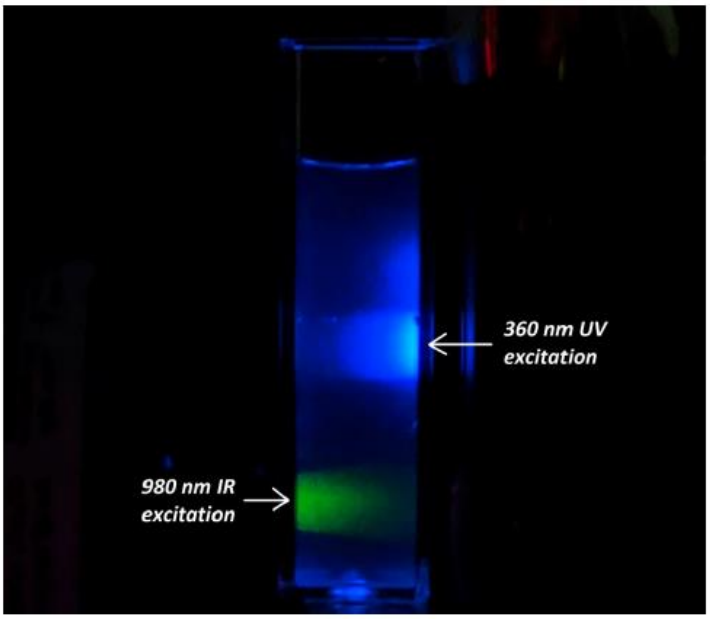

Figure 38. Blue fluorescence emission from Stilebene-420 under 360 nm UV excitation and green emission from upconverting particles when excited by 980 nm. Reprinted with permission from (50).

Eyeglass device

Figure 39 shows images recorded by a camera behind the eyepiece lens of the device. The upconverting screen consisted of a glass slide coated with upconverting particles. The intensity of the 980 nm IR light was ~500 mW/cm^2, whereas that of the visible and UV light were ~1 mW/cm^2.

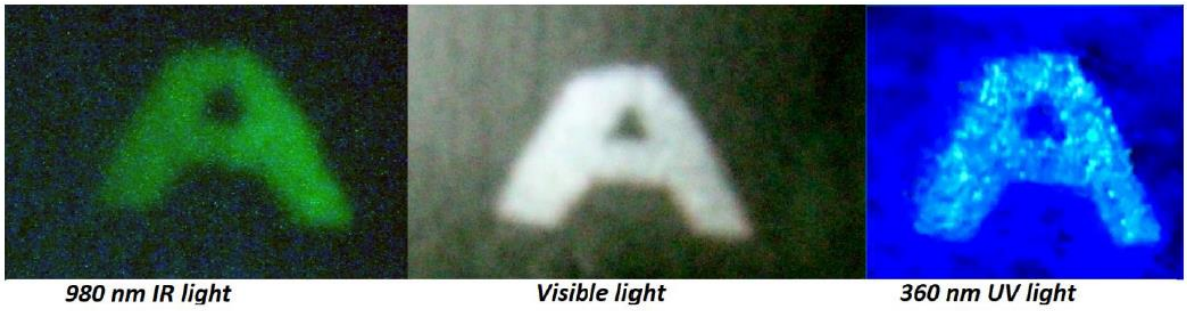

Figure 39. Images recorded by the constructed device under 980 nm IR, visible, and 360 nm UV light illumination. Reprinted with permission from (50).

These data suggest, rather strongly, that the upconverting microparticles are strong candidates for increasing the visual range to the near IR, while Stilbene-420 dye and GFP are good candidates for extending the visual range to the near UV. We are continuing this research and have designed means for increasing the IR to visible upconversion efficiency.

CHAPTER V

CONCLUSION

In this work, thymine dimers were detected spectroscopically, for the first time, in thymine and DNA solutions, using Raman spectroscopy. It was shown that the formation of thymine dimers continues to increase, upon UV irradiation, for 20 minutes, and then becomes constant due to the formation of equilibrium between thymine dimers and monomers. A hand-held instrument based on resonance Raman spectroscopy was designed, constructed, and used to identify different bacterial strains. Another hand-held instrument, using a cell-phone camera as a detector, was built and the Raman spectra of different molecules were recorded. In our previous studies, we have shown that the fluorescence intensities of tryptophan and tyrosine components of bacteria decrease as a function of UV irradiation. In this study, we have used this principle to design and construct a portable device that can remotely record the fluorescence of bacteria and record the decrease in fluorescence intensity as a function of UV irradiation. Lastly, we constructed an eye-ware device, which consists of a screen with upconverting microparticles dispersed on it along with UV to visible converting dye. This device can be used to expand the human visual range from near-IR to near-UV.

REFERENCES

1. B. Aslam *et al.*, Antibiotic resistance: a rundown of a global crisis. *Infect Drug Resist* **11**, 1645-1658 (2018).
2. CDC, Antibiotic resistance threats in the United States, 2019. (2019).
3. D. J. Weber, R. Raasch, W. A. Rutala, Nosocomial infections in the ICU: the growing importance of antibiotic-resistant pathogens. *Chest* **115**, 34S-41S (1999).
4. R. Beukers, J. Ijlstra, W. Berends, The effect of ultraviolet light on some components of the nucleic acids. VI The origin of the U.V. sensitivity of deoxyribonucleic acid. *Recueil des Travaux Chimiques des Pays-Bas* **79**, 101-104 (1960).
5. R. Li, D. Dhankhar, J. Chen, T. C. Cesario, P. M. Rentzepis, A tryptophan synchronous and normal fluorescence study on bacteria inactivation mechanism. *Proc Natl Acad Sci U S A* **116**, 18822-18826 (2019).
6. Anonymous, Ancient bacteria alive and well. *Trends in Microbiology* **9**, 12 (2001).
7. R. M. Macnab, Genetics and biogenesis of bacterial flagella. *Annu Rev Genet* **26**, 131-158 (1992).
8. R. Fronzes, H. Remaut, G. Waksman, Architectures and biogenesis of non-flagellar protein appendages in Gram-negative bacteria. *EMBO J* **27**, 2271-2280 (2008).
9. J. P. Duguid, I. W. Smith, G. Dempster, P. N. Edmunds, Non-flagellar filamentous appendages (fimbriae) and haemagglutinating activity in Bacterium coli. *J Pathol Bacteriol* **70**, 335-348 (1955).
10. R. Lowry, S. Balboa, J. L. Parker, J. G. Shaw, "Chapter Five - Aeromonas Flagella and Colonisation Mechanisms" in Advances in Microbial Physiology, R. K. Poole, Ed. (Academic Press, 2014), vol. 65, pp. 203-256.

11. W. Vollmer, D. Blanot, M. A. de Pedro, Peptidoglycan structure and architecture. *FEMS Microbiol Rev* **32**, 149-167 (2008).

12. H. Strahl, J. Errington, Bacterial Membranes: Structure, Domains, and Function. *Annu Rev Microbiol* **71**, 519-538 (2017).

13. M. Nomura, Bacterial ribosome. *Bacteriol Rev* **34**, 228-277 (1970).

14. Anonymous, *Medical Microbiology. 4th Edition* (University of Texas Medical Branch at Galveston., 1996).

15. C. L. Ventola, The antibiotic resistance crisis: part 1: causes and threats. *P T* **40**, 277-283 (2015).

16. D. L. Wulff, G. Fraenkel, On the nature of thymine photoproduct. *Biochimica et Biophysica Acta* **51**, 332-339 (1961).

17. R. B. Setlow, J. K. Setlow, Evidence that ultraviolet-induced thymine dimers in DNA cause biological damage. *Proc Natl Acad Sci U S A* **48**, 1250-1257 (1962).

18. R. B. Setlow, Cyclobutane-type pyrimidine dimers in polynucleotides. *Science* **153**, 379-386 (1966).

19. A. J. Varghese, S. Y. Wang, Thymine-thymine adduct as a photoproduct of thymine. *Science* **160**, 186-187 (1968).

20. K. Sofinska, N. Wilkosz, M. Szymonski, E. Lipiec, Molecular Spectroscopic Markers of DNA Damage. *Molecules* **25**, 561 (2020).

21. T. Douki, J. Cadet, Individual determination of the yield of the main UV-induced dimeric pyrimidine photoproducts in DNA suggests a high mutagenicity of CC photolesions. *Biochemistry* **40**, 2495-2501 (2001).

22. H. Yokoyama, R. Mizutani, Structural biology of DNA (6-4) photoproducts formed by ultraviolet radiation and interactions with their binding proteins. *Int J Mol Sci* **15**, 20321-20338 (2014).

23. P. H. Clingen, R. J. H. Davies, Quantum yields of adenine photodimerization in poly(deoxyadenylic acid) and DNA. *J Photoch Photobio B* **38**, 81-87 (1997).

24. A. Nagpal *et al.*, Thymine dissociation and dimer formation: A Raman and synchronous fluorescence spectroscopic study. *Proc Natl Acad Sci U S A* **118**, e2025263118 (2021).

25. S. Y. Wang, Photochemical Reactions in Frozen Solutions. *Nature* **190**, 690-+ (1961).

26. S. Y. Wang, The Mechanism for Frozen Aqueous Solution Irradiation of Pyrimidines. *Photochemistry and Photobiology* **3**, 395-398 (1964).

27. A. Smekal, Zur Quantentheorie der Dispersion. *Naturwissenschaften* **11**, 873-875 (1923).

28. C. V. Raman, K. S. Krishnan, A new type of secondary radiation. *Nature* **121**, 501-502 (1928).

29. D. P. Strommen, K. Nakamoto, Resonance Raman-Spectroscopy. *Journal of Chemical Education* **54**, 474-478 (1977).

30. N. Bloembergen, Solid State Infrared Quantum Counters. *Physical Review Letters* **2**, 84-85 (1959).

31. F. Auzel, Upconversion and anti-Stokes processes with f and d ions in solids. *Chem Rev* **104**, 139-173 (2004).

32. X. Wen, P. Yu, Y. R. Toh, X. Ma, J. Tang, On the upconversion fluorescence in carbon nanodots and graphene quantum dots. *Chem Commun (Camb)* **50**, 4703-4706 (2014).

33. E. Poles, D. C. Selmarten, O. I. Micic, A. J. Nozik, Anti-Stokes photoluminescence in colloidal semiconductor quantum dots. *Applied Physics Letters* **75**, 971-973 (1999).

34. S. A. Blanton, M. A. Hines, P. GuyotSionnest, Photoluminescence wandering in single CdSe nanocrystals. *Applied Physics Letters* **69**, 3905-3907 (1996).

35. H. Dong *et al.*, Lanthanide Nanoparticles: From Design toward Bioimaging and Therapy. *Chem Rev* **115**, 10725-10815 (2015).

36. A. Sedlmeier, H. H. Gorris, Surface modification and characterization of photon-upconverting nanoparticles for bioanalytical applications. *Chem Soc Rev* **44**, 1526-1560 (2015).

37. O. S. Wolfbeis, An overview of nanoparticles commonly used in fluorescent bioimaging. *Chem Soc Rev* **44**, 4743-4768 (2015).

38. B. M. van der Ende, L. Aarts, A. Meijerink, Lanthanide ions as spectral converters for solar cells. *Phys Chem Chem Phys* **11**, 11081-11095 (2009).

39. C. Yuan *et al.*, Simultaneous multiple wavelength upconversion in a core-shell nanoparticle for enhanced near infrared light harvesting in a dye-sensitized solar cell. *ACS Appl Mater Interfaces* **6**, 18018-18025 (2014).

40. S. Hao, G. Chen, C. Yang, Sensing using rare-earth-doped upconversion nanoparticles. *Theranostics* **3**, 331-345 (2013).

41. J. Hampl *et al.*, Upconverting phosphor reporters in immunochromatographic assays. *Anal Biochem* **288**, 176-187 (2001).

42. P. Zhang, S. Rogelj, K. Nguyen, D. Wheeler, Design of a highly sensitive and specific nucleotide sensor based on photon upconverting particles. *J Am Chem Soc* **128**, 12410-12411 (2006).

43. A. Baride *et al.*, A NIR-to-NIR upconversion luminescence system for security printing applications. *Rsc Advances* **5**, 101338-101346 (2015).

44. J. C. Bunzli, C. Piguet, Taking advantage of luminescent lanthanide ions. *Chem Soc Rev* **34**, 1048-1077 (2005).

45. N. Menyuk, K. Dwight, J. W. Pierce, NaYF4: Yb,Er—an efficient upconversion phosphor. *Applied Physics Letters* **21**, 159-161 (1972).

46. D. Dhankhar *et al.*, Resonance Raman Spectra for the In Situ Identification of Bacteria Strains and Their Inactivation Mechanism. *Appl Spectrosc* 10.1177/0003702821992834, 3702821992834 (2021).

47. D. Dhankhar, A. Nagpal, P. M. Rentzepis, Cell-phone camera Raman spectrometer. *Review of Scientific Instruments* **92**, 054101 (2021).

48. D. Dhankhar *et al.*, A novel approach for remote detection of bacteria using simple charge-coupled device cameras and telescope. *Rev Sci Instrum* **91**, 074106 (2020).

49. J. C. Boyer, F. C. van Veggel, Absolute quantum yield measurements of colloidal NaYF4: Er3+, Yb3+ upconverting nanoparticles. *Nanoscale* **2**, 1417-1419 (2010).

50. D. Dhankhar *et al.*, Extending Human Vision to Infrared and Ultraviolet Light: A Study Using Micro-Particles and Fluorescent Molecules. *Ieee Access* **8**, 73890-73897 (2020).

51. J. S. Singh, FTIR and Raman spectra and fundamental frequencies of biomolecule: 5-methyluracil (thymine). *Journal of Molecular Structure* **876**, 127-133 (2008).

52. K. Szczepaniak, M. M. Szczesniak, W. B. Person, Raman and infrared spectra of thymine. A matrix isolation and DFT study. *J Phys Chem A* **104**, 3852-3863 (2000).

53. S. L. Zhang, K. H. Michaelian, G. R. Loppnow, Vibrational spectra and experimental assignments of thymine and nine of its isotopomers. *J Phys Chem A* **102**, 461-470 (1998).

54. S. N. Bose, R. J. Davies, S. K. Sethi, J. A. McCloskey, Formation of an adenine-thymine photoadduct in the deoxydinucleoside monophosphate d(TpA) and in DNA. *Science* **220**, 723-725 (1983).

55. B. Prescott, W. Steinmetz, G. J. Thomas, Jr., Characterization of DNA structures by laser Raman spectroscopy. *Biopolymers* **23**, 235-256 (1984).

56. F. D'Amico *et al.*, Oxidative damage in DNA bases revealed by UV resonant Raman spectroscopy. *Analyst* **140**, 1477-1485 (2015).

57. S. L. Jensen, Biosynthesis and function of carotenoid pigments in microorganisms. *Annu Rev Microbiol* **19**, 163-182 (1965).

58. N. I. Krinsky, Non-Photosynthetic Functions of Carotenoids. *Philos T Roy Soc B* **284**, 581-590 (1978).

59. P. Rosch *et al.*, Chemotaxonomic identification of single bacteria by micro-Raman spectroscopy: application to clean-room-relevant biological contaminations. *Appl Environ Microbiol* **71**, 1626-1637 (2005).

60. W. E. Huang, R. I. Griffiths, I. P. Thompson, M. J. Bailey, A. S. Whiteley, Raman microscopic analysis of single microbial cells. *Anal Chem* **76**, 4452-4458 (2004).

61. P. Rosch *et al.*, Identification of single eukaryotic cells with micro-Raman spectroscopy. *Biopolymers* **82**, 312-316 (2006).

62. J. Jehlicka, H. G. Edwards, A. Oren, Raman spectroscopy of microbial pigments. *Appl Environ Microbiol* **80**, 3286-3295 (2014).

63. T. Yammoto, G. Palmer, The valence and spin state of iron in oxyhemoglobin as inferred from resonance Raman spectroscopy. *J Biol Chem* **248**, 5211-5213 (1973).

64. V. Kumar, B. Kampe, P. Rosch, J. Popp, Classification and identification of pigmented cocci bacteria relevant to the soil environment via Raman spectroscopy. *Environ Sci Pollut Res Int* **22**, 19317-19325 (2015).